

**Acoustic Emission Instrumentation System for  
Monitoring Large Superconducting Magnets**

by  
Kenneth Dylan Jacob

B.I.S., University of Minnesota  
(1981)

Submitted to the Department of  
Mechanical Engineering  
in Partial Fulfillment of the  
Requirements of the Degree of

MASTER OF SCIENCE

at the

MASSACHUSETTS INSTITUTE OF TECHNOLOGY

January 1984

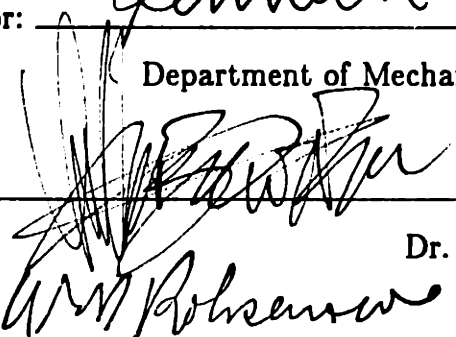
© Massachusetts Institute of Technology, 1984

Signature of Author: \_\_\_\_\_



Department of Mechanical Engineering, 20 January 1984

Certified by: \_\_\_\_\_



Dr. Yukikazu Iwasa, Thesis Supervisor

Accepted by: \_\_\_\_\_



Chairman, Mechanical Engineering Departmental Committee

MASSACHUSETTS INSTITUTE  
OF TECHNOLOGY

Archives

MAR 21 1984

LIBRARIES

# **Acoustic Emission Instrumentation System for Monitoring Large Superconducting Magnets**

by  
Kenneth Dylan Jacob

Submitted to the Department of Mechanical Engineering  
on January 20, 1984 in partial fulfillment of the  
requirements for the Degree of Master of Science

## **ABSTRACT**

An Acoustic Emission (AE) instrumentation system has been developed for monitoring large superconducting magnet systems. This new system permits AE signal recording with improved signal-to-noise ratios and makes possible the development and use of more sophisticated data analysis techniques.

The system has been designed to monitor some of the six superconducting magnets being assembled at the Oak Ridge National Laboratory under the U.S. Department of Energy Large Coil Program (LCP). Installation, calibration, and testing of the AE system on one of the LCP coils is described.

In addition, results of experiments designed to enhance the understanding of the propagation of AE signals in superconducting magnets are presented. Finally, work currently being conducted towards improving the acquisition and analysis of AE data is outlined.

**Thesis Supervisor: Dr. Yukikazu Iwasa**

**Title: Senior Research Engineer, Francis Bitter National Magnet Laboratory and  
Department of Mechanical Engineering**

# Table of Contents

|   |    |
|---|----|
| Title . . . . .   | 1  |
| Abstract . . . . .  | 2  |
| Dedication and Acknowledgements . . . . .                   | 6  |
| <br>  |    |
| 1. Introduction . . . . .                                   | 7  |
| 1.1. Superconductors and Superconducting Magnets . . . . .  | 7  |
| 1.2. Acoustic Emission . . . . .                            | 8  |
| 1.3. Acoustic Emission in Superconducting Magnets . . . . . | 9  |
| 1.3.1. Early Qualitative Observations . . . . .             | 9  |
| 1.3.2. Sources of Acoustic Emission . . . . .               | 10 |
| 1.3.3. Location of Sources of Acoustic Emission . . . . .   | 12 |
| 1.3.4. Large Scale Applications . . . . .                   | 14 |
| 1.4. Thesis Objectives . . . . .                            | 14 |
| 2. AE Instrumentation System . . . . .                      | 18 |
| 2.1. Acoustic Emission Sensors . . . . .                    | 18 |
| 2.2. Unique AE Sensor Design . . . . .                      | 20 |
| 2.3. Differential Sensor . . . . .                          | 21 |
| 2.3.1. Concept of the Differential Sensor . . . . .         | 21 |
| 2.3.2. Construction of the Differential Sensor . . . . .    | 22 |
| 2.4. Sensor Testing and Calibration . . . . .               | 22 |
| 2.4.1. Absolute Calibration . . . . .                       | 22 |
| 2.4.2. Relative Calibration . . . . .                       | 24 |
| 2.5. Effects of Clamping . . . . .                          | 30 |
| 2.6. Effects of Mylar . . . . .                             | 32 |
| 2.7. Effects of Temperature . . . . .                       | 34 |
| 2.8. Differential Amplifier . . . . .                       | 35 |
| 2.9. Secondary Amplifier . . . . .                          | 36 |
| 2.10. Multi-Channel Tape Recorder . . . . .                 | 37 |

|  |    |
|--|----|
| 2.11. Waveform Digitizer . . . . .                                 | 38 |
| 2.12. Sensor Guards . . . . .                                      | 39 |
| 3. Large Coil Program Data Acquisition . . . . .                   | 40 |
| 3.1. Large Coil Program (LCP) . . . . .                            | 40 |
| 3.2. Large Coil Test Facility . . . . .                            | 41 |
| 3.3. General Dynamics LCP Coil . . . . .                           | 41 |
| 3.4. AE Program Objectives . . . . .                               | 41 |
| 3.4.1. Classification of AE Events . . . . .                       | 42 |
| 3.4.2. Event Localization . . . . .                                | 42 |
| 3.5. Sensor Installation . . . . .                                 | 43 |
| 3.6. Sensor Locations . . . . .                                    | 43 |
| 3.7. System Calibration . . . . .                                  | 46 |
| 3.7.1. Phase One . . . . .   | 46 |
| 3.7.2. Phase Two . . . . .   | 47 |
| 3.8. GD System Calibration Results . . . . .                       | 47 |
| 3.8.1. Sensor Response . . . . .                                   | 47 |
| 3.8.2. Wave Speed . . . . .  | 50 |
| 3.8.3. Signal Attenuation and Broadening . . . . .                 | 51 |
| 3.8.4. Frequency Analysis . . . . .                                | 55 |
| 4. Data Processing and Analysis . . . . .                          | 62 |
| 4.1. Wave Propagation Research . . . . .                           | 62 |
| 4.1.1. Wavefront Propagation in a "Pancake" Winding . . . . .      | 62 |
| 4.1.2. Attenuation of High Frequencies in Magnet Winding . . . . . | 65 |
| 4.1.3. Discussion of Results . . . . .                             | 65 |
| 4.2. LCP Data Analysis Recommendations . . . . .                   | 67 |
| 4.3. Signal Processing Recommendations . . . . .                   | 68 |
| 4.3.1. Analog Signal Processing . . . . .                          | 68 |
| 4.3.2. Analog/Digital Signal Processing . . . . .                  | 69 |
| 4.3.3. Development of Analog/Digital Signal Processor . . . . .    | 70 |
| 4.3.4. Software-Based Data Analysis . . . . .                      | 71 |
| 5. Summary and Conclusions . . . . .                               | 73 |

|   |           |
|---|-----------|
| <b>6. Appendices</b> . . . . .  | <b>74</b> |
| <b>6.1. Appendix A: Differential Sensor Construction</b> . . . . .    | <b>74</b> |
| <b>6.2. Appendix B: Secondary Amplifier Circuit Diagram</b> . . . . . | <b>76</b> |
| <b>6.3. Appendix C: General Dynamics LCP Coil</b> . . . . .           | <b>77</b> |
| <b>6.4. Appendix D: GD Sensor Coordinates</b> . . . . .               | <b>79</b> |
| <b>6.5. Appendix E: Pancake Coil Parameters</b> . . . . .             | <b>81</b> |
| <b>6.5. Appendix F: LCTF Feedthrough Plug Configuration</b> . . . . . | <b>82</b> |

## **Dedication**

To my family, whose support has made this possible,  
and to Ann, who I love.

## **Acknowledgements**

I would like to acknowledge the entire staff of the Plasma Fusion Center and the Francis Bitter National Magnet Laboratory for their support. In particular, for the guidance, counseling and friendship of my thesis supervisor, Yukikazu Iwasa. For her friendship, understanding, and interest in sports, Barbara Keesler. For his technical expertise and advice, David Johnson. And to Albe Dawson, who has proofread everything I have written here.

In addition, I would like to acknowledge Professor Amar Bose, whose approach to teaching and engineering science should not be unique at MIT. He and Yuki have been largely responsible for making the whole thing fun.

This work was supported in part by the Office of Fusion Energy, Department of Energy and in part by the National Science Foundation.

# 1. INTRODUCTION

## 1.1. Superconductors and Superconducting Magnets

Superconductors are materials which, when kept at temperatures near absolute zero, conduct electricity with no resistance. Superconducting devices are improvements over their predecessors constructed from normal resistive conductors for several reasons: 1) power is necessary only for the refrigeration of the conductor and 2) the higher current densities possible in superconductors allow the devices to be compact.

Electromagnets were obvious choices for the use of superconductors since high magnetic fields could be produced efficiently and with smaller bulk. Superconducting magnets have been developed and constructed for a wide variety of applications, including magnets for magnetohydrodynamic (MHD) power generation, nuclear magnetic resonance (NMR) technology, and particle accelerators used in high energy physics applications. Superconducting magnets necessary for magnetic confinement of plasmas for controlled nuclear fusion devices are the focus of extensive research and development efforts in the U.S., the Soviet Union, Japan, and Europe, and represent one of the large-scale applications of superconducting technology.

Ensuring the safety, reliability, endurance, and proper performance of superconducting magnet systems makes necessary the development of new diagnostic techniques and instrumentation. Some issues unique to these systems which emphasize this need include:

- (1) Superconducting magnet technology is comparatively young, and experience in magnet construction and operation is limited.
- (2) In the presence of current and magnetic field, superconductors can operate only in a narrow temperature range, usually a few degrees, and are therefore susceptible to quench (sudden loss of superconductivity) when subjected to very small amounts of localized energy in the form of heat. The extreme forces acting on the magnet and its support structure can cause mechanical disturbances which release sufficient heat to drive the conductor normal, or nonsuperconducting. Strategies for preventing

or controlling these perturbations will rely on diagnostic techniques capable of sensing and characterizing the disturbances.

- (3) The magnetically-coupled energy transfer system in a superconducting magnet may enable its total stored energy to be dissipated over a small winding region, possibly causing a local burn-out of the superconductor.
- (4) There are associated with large magnets complicated structural and cryogenic systems whose integrity must be ensured. These include support structures and magnet windings subject to enormous forces and wide ranges of temperature and pressure.

Superconducting magnet systems, especially those comprising subunits of a larger system, must be protected over the entire lifetime of the system, requiring instrumentation and data processing systems capable of recognizing both long and short term trends in magnet behavior. These issues indicate the need for a battery of diagnostic techniques capable of monitoring and in some cases predicting magnet behavior.

## **1.2. Acoustic Emission**

*Acoustic Emission (AE)* is a term used to describe the acoustic signals emitted by materials and structures. These signals can be either periodic signals or discrete events. Simple examples of AE are the squeaking sound a bicycle wheel makes when an axle bearing is worn or loose (periodic emission) or the cracking noise a piece of wood makes as it is bent (discrete event emission). AE can signify both normal operation of a dynamic system — say the sound of a lawnmower — and abnormal operation — when the lawnmower blade hits a rock.

*Acoustic emission monitoring* refers to the process of sensing and analyzing acoustic signals. It is analogous to a physician using a stethoscope to listen to and diagnose a patient. AE monitoring has been used in a variety of industrial applications, some of which are:

- 1) Crack detection, location, and propagation in pressure vessels.



- 2) Leak detection and location.
- 3) Weld monitoring.
- 4) Semiconductor manufacturing.
- 5) Determination of structural integrity.
- 6) Material strength testing.
- 7) Orthopedic applications.

AE monitoring techniques have proven to be particularly useful in detecting and locating small mechanical disturbances in large structures. For example, the acoustic stress waves emitted by a small crack in the underwater support structure of an offshore oil platform — smaller than can be detected visually by divers, but large enough to be potentially hazardous — might be sensed over one hundred feet away on the same structure by AE sensors, the location of the crack determined, and the crack's size estimated. This example illustrates several key features of AE monitoring techniques: 1) modern AE transducers are sensitive enough to detect stress waves from mechanical disturbances too small to be detected by other methods, 2) large structures can be monitored with relatively few strategically placed sensors, and 3) arrival time differences of AE signals on an array of sensors can be used to triangulate (locate) the source of the disturbance. These features make AE monitoring a potentially attractive diagnostic tool for monitoring superconducting magnets.

### **1.3. Acoustic Emission in Superconducting Magnets**

#### **1.3.1. Early Qualitative Observations**

Microphones, accelerometers, and human ears were originally used to monitor a variety of noises produced by superconducting magnets during charging. Also recorded was the so-called Kaiser effect, where AE signals appeared only after the current level in a magnet charging sequence exceeded the level reached in the previous sequence.<sup>1</sup>

---

<sup>1</sup>H. Nomura, et.al., "Acoustic emission from superconducting magnets," *Cryogenics*, 17, 471 (1977).

Nomura et al,<sup>1</sup> made further qualitative observations based on AE data from superconducting magnets. These included: 1) the frequency and magnitude of AE events increased with increasing magnetic field, 2) a strong AE burst occurred at the time of a magnet quench, and 3) no AE occurred at constant current and magnetic field.

These experiments offered evidence that AE had potential as a diagnostic technique; work began at this laboratory in 1978 to develop AE techniques for monitoring superconducting magnets.

### 1.3.2. Sources of Acoustic Emission

It was known that superconducting magnets generated acoustic signals in the form of impulsive events,<sup>1</sup> but the source, or sources, of these emissions remained to be determined. Speculation centered on the following possibilities:<sup>2</sup>

- (1) Straining of the superconductor.
- (2) Straining of the magnet structure.
- (3) The vibrations caused when bundles of fluxoids in the superconductor are forcibly depinned by Lorentz force interaction of the magnetic field and transport current, called flux motion or flux jumping.
- (4) Motion of the conductor.
- (5) Bursting of liquid helium bubbles.

As the concentration of titanium is increased in a niobium-titanium (NbTi) superconductor, the number of flux pinning centers also increases.<sup>3</sup> Pasztor and Schmidt<sup>4</sup> had observed an increase in AE counting rates with an increase in the titanium concentration and hypothesized that acoustic signals were being produced by flux jumping. They were unable, however, to produce any experimental proof that such flux jumps occurred and that the jumps produced acoustic signals.

<sup>2</sup>For a detailed discussion see O. Tsukamoto, and Y. Iwasa, "Sources of acoustic emission in superconducting magnets," *J. Appl. Phys.* **51**, 997 (1983).

<sup>3</sup>J.E.C. Williams, Superconductivity and its Applications, Pion Limited, London, 1970.

<sup>4</sup>G. Pasztor and C. Schmidt, "Acoustic emission from NbTi superconductors during flux jump," *Cryogenics*, **19**, 608 (1979).

Nomura, Sinclair, and Iwasa<sup>5</sup> observed that a sharp increase in the AE counting rate occurred as the current in a sample superconductor neared its critical value. They believed that flux jumping should be most rapid in the transition of the conductor from its superconducting to its normal state and were able to explain their data in part by using Bean's magnetization model.<sup>6</sup> Hence there was some further reason to believe that flux jumping was responsible for producing acoustic signals.

In each of these experiments, however, signals from AE sensors were badly corrupted by various forms of noise, calling into question the validity of some of the results. In addition, Tsukamoto<sup>2</sup> later showed that the energy released by flux jumping was significantly lower than that contained in observed AE events.

In retrospect, two earlier experiments were pointing to conductor motion as being a source of acoustic emission. First, Turowski<sup>7</sup> observed the near coincidence of a voltage transient and an AE event just prior to a premature magnet quench but found that the AE signal was absent when the magnet quenched upon reaching its critical current. Second, Kensley, Maeda, and Iwasa<sup>8</sup> observed AE from slipping surfaces of a superconductor, indicating that mechanical motion in superconductors could cause AE.

Experiments were designed to test the hypothesis that conductor motion was a source of AE in superconducting magnets, and that conductor motion events are accompanied by a voltage transient. One experiment<sup>9</sup> compared the number of AE events for two situations: 1) where a superconductor was free to move against a solid phenolic cylinder, and 2) where the superconductor was firmly potted to the cylinder with epoxy. In each case, the cylinder was placed in a magnetic field causing sideways forces to act on the superconducting wire. It was found that AE was present only when the conductor was free to move. In addition, a model was developed showing that the

<sup>5</sup>H. Nomura, M.W. Sinclair, and Y. Iwasa, "Acoustic emission in a composite Copper NbTi conductor," *Cryogenics*, 20, 283 (1980).

<sup>6</sup>C.P. Bean, "Magnetization of Hard Superconductors," *Phys. Rev. Lett.*, 8, 250 (1962).

<sup>7</sup>P. Turowski, "Acoustic emission and flux jump phenomena during training of superconducting magnets," *Proc. Sixth Int'l Conf. on Magnet Technology (MT-6)*, (Alfa Press, Bratislava) 648 (1978).

<sup>8</sup>R.S. Kensley, H. Maeda, and Y. Iwasa, "Transient slip behavior of metal/insulator pairs at 4.2 K," *Cryogenics*, 21, 479 (1981).

<sup>9</sup>O. Tsukamoto, M.W. Sinclair, M.F. Steinhoff, and Y. Iwasa, "Origins of acoustic emission in superconducting wires," *Appl. Phys. Lett.* 38, 718 (1981).

energy released by the wire movement was compatible with the energy contained in the AE signals. In a similar experiment,<sup>10</sup> premature magnet quenches resulted from induced conductor motion, and an accompanying AE event and voltage transient were observed (Figure 1), demonstrating that conductor motion was responsible for some premature magnet quenches and that AE instrumentation could be used to monitor these critical motions.

Data<sup>11,12</sup> from several large superconducting magnets have shown a great number of conductor-motion-induced AE events; however, a great many events were not accompanied by a voltage transient. These have been lumped into the general category of structural AE events, although it is assumed that the signals are originating from a variety of sources not strictly structural in origin. For example, recent experiments<sup>13</sup> suggest that epoxy used to pot the conductors cracks and causes a "structural" AE event. It is partially within the scope of the work described here to develop techniques to identify these sources of structural AE.

### 1.3.3. Location of Sources of Acoustic Emission

Tsukamoto and Iwasa<sup>14</sup> designed a simple experiment in which three AE sensors could triangulate the source of a conductor motion event. Stress wave propagation velocity was measured and correlated with time delays between initiation of an AE event on each of the three sensors. The simple linear geometry of the sample holder allowed the source of the event to be determined to a high degree of accuracy. The experiment was designed to demonstrate the feasibility of a triangulation technique; such a technique applied to a large superconducting magnet would require many more sensors and an understanding of stress wave propagation paths and speeds in the

---

<sup>10</sup>O. Tsukamoto, J.F. Maguire, E.S. Bobrov, and Y. Iwasa, "Identification of quench origins in a superconductor with acoustic emission and voltage measurements," *Appl. Phys. Lett.* **39**, 172 (1981).

<sup>11</sup>O. Tsukamoto, M.F. Steinhoff, and Y. Iwasa, "Acoustic emission triangulation of mechanical disturbances in superconducting magnets," *Proceedings of the 9th Symp. on Eng. Problems of Fusion Research*, (IEEE Pub. No. 81CH1715-2 NPS) 309 (1981).

<sup>12</sup>J. Lore, N. Tamada, O. Tsukamoto, and Y. Iwasa, "Acoustic emission monitoring results from the MFTF magnets," [to appear in *Cryogenics* (1984)].

<sup>13</sup>Results of experiments conducted in this laboratory will be submitted for publication.

<sup>14</sup>O. Tsukamoto, and Y. Iwasa, "Acoustic emission triangulation of disturbances and quenches in a superconductor and a superconducting magnet," *Appl. Phys. Lett.*, **40**, 538 (1982).

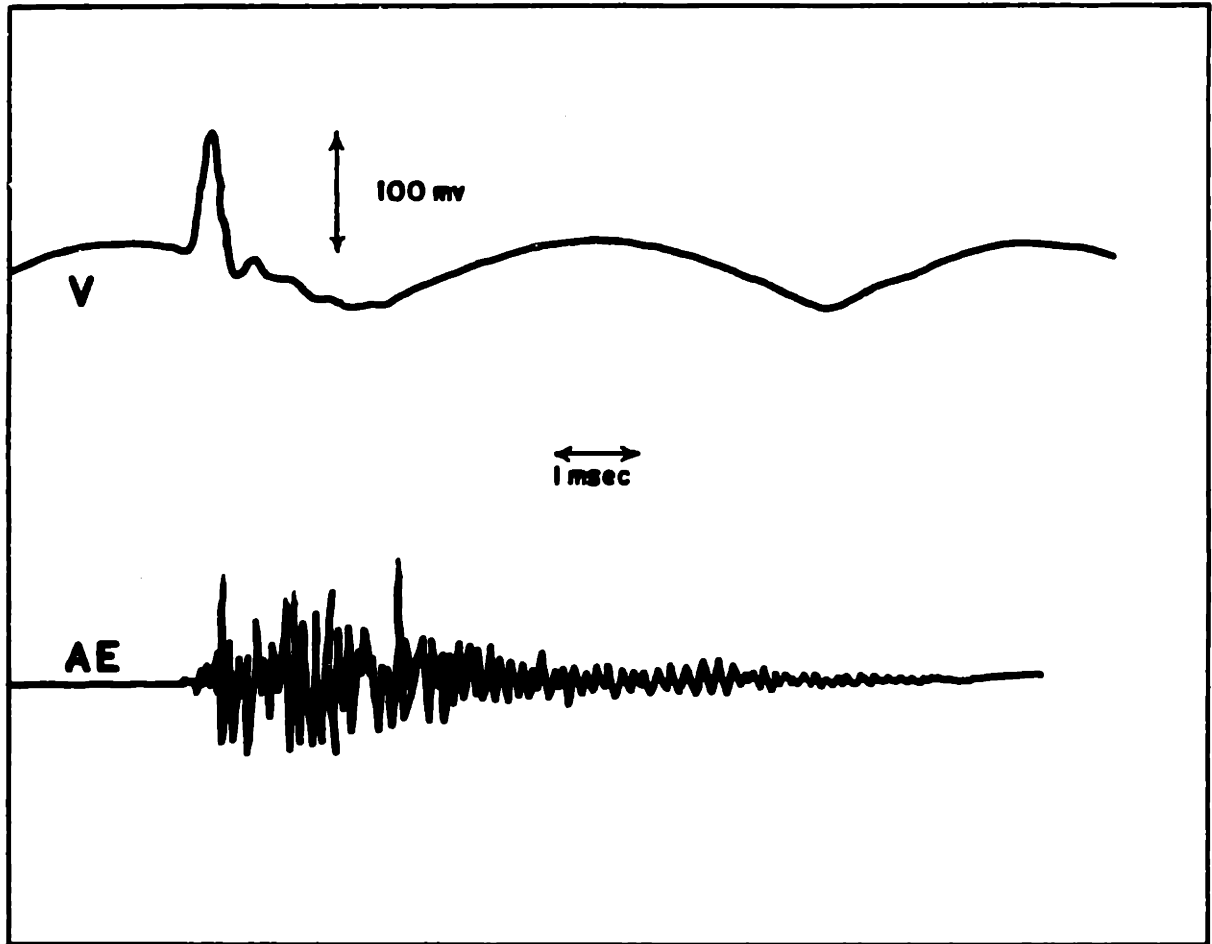


Fig. 1 Coincidence AE burst (top trace) and voltage transient (bottom trace).<sup>2</sup>

magnet. This problem is the subject of current research in this laboratory and some experimental results are presented later (see section 4.1.).

#### **1.3.4. Large-Scale Applications**

Over the past two years, data have been taken from several large superconducting magnets. Sensors placed on the Brookhaven National Laboratory's Isabelle Colliding Beam Accelerator dipoles localized the source of coil quench to conductor motion in the end turns of the magnet.<sup>11</sup> Similarly, conductor motions were identified in the 170-ton MHD magnet at the Argonne National Laboratory.<sup>11</sup>

Most recently, data from twelve sensors placed on the huge MFTF-B yin-yang magnet coils at the Lawrence Livermore National Laboratory were analyzed using an MIT-designed and built signal processor, capable of distinguishing between conductor motion and other AE events.<sup>12</sup> The device used an analog-to-digital converter to read and code AE data from the tape recordings made during magnet charging sequences. The digitally-coded information was then passed to a PDP-11/23 minicomputer, where it was stored, and later analyzed and plotted. An example of the computer-processed plots is shown in Figure 2.

#### **1.4. Thesis Objectives**

1) One of the recurring and most troublesome problems with AE data from superconducting magnets has been the presence of noise. Past data acquisition systems have been particularly susceptible to noise generated by the magnet's power supply, and a series of superimposed periodic spikes usually resulted. This was the case with recordings of AE signals from the MFTF magnet, and it became necessary to design and build a special signal processing circuit capable of recognizing and filtering the noise.

2) Another predominant problem with past systems is the great difference in sensitivity between the several sensor circuits. Furthermore, no simple, repeatable, and accurate means of calibrating the system was developed. The result is analog AE recordings where AE event amplitudes are virtually meaningless, and where a great many data may be lost because of weak sensors. One objective of the work described here has been, therefore, to design, build, and test a new AE data acquisition system

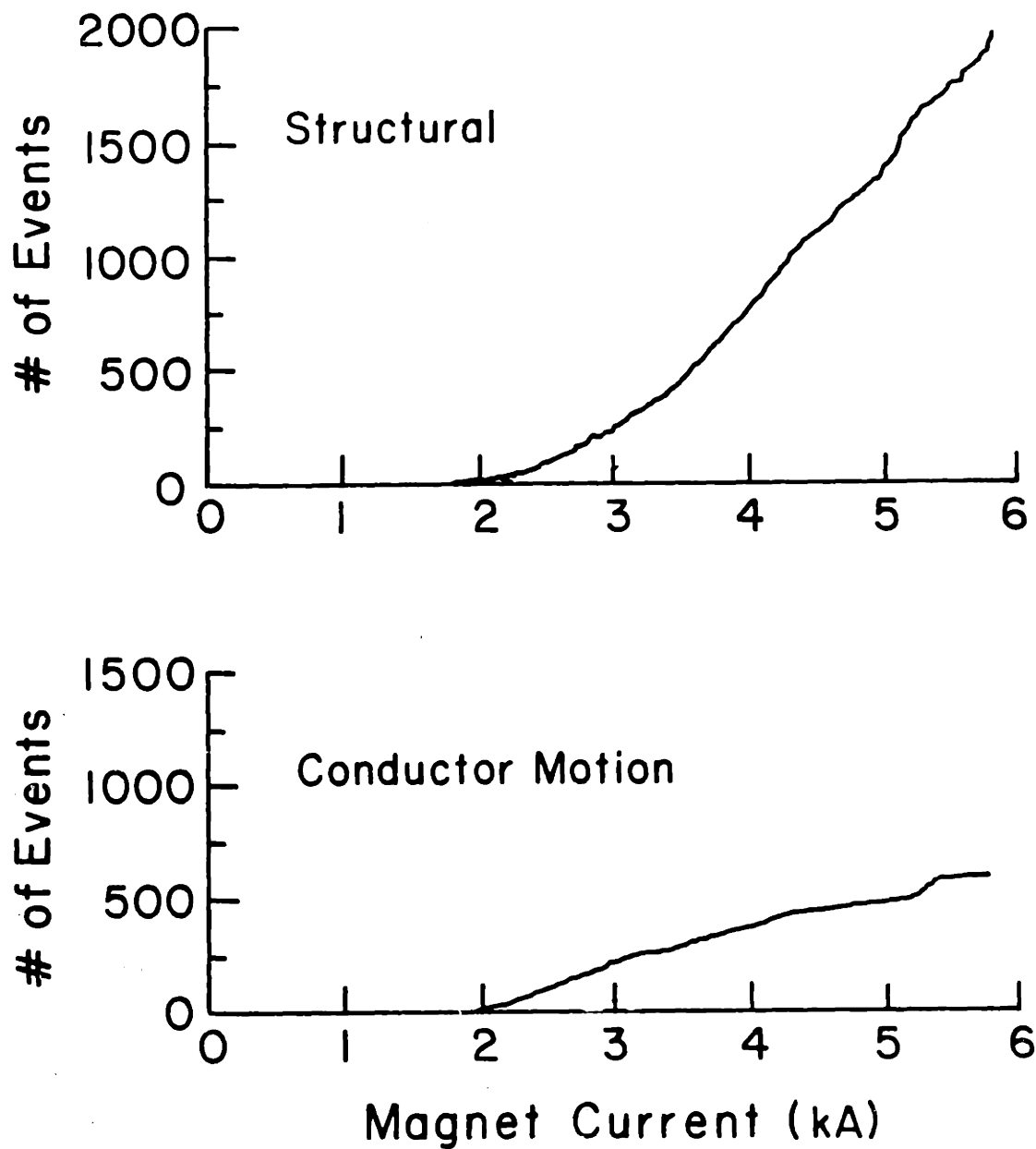


Fig. 2 Example of computer-processed plots showing AE activity *vs.* magnet current.<sup>17</sup>

that is both resistant to the forms of noise that have plagued past systems and can be calibrated. Each component in the new system will be described and where applicable, results from its calibration and testing will be presented.

3) Another objective has been the implementation of the new instrumentation system on the General Dynamics (GD) fusion test magnet, one of six coils making up the Large Coil Program (LCP) at the Oak Ridge National Laboratory. Figure 3 shows a schematic view of the magnets and their support structure. In addition to providing an excellent opportunity to install the fully assembled system on a large scale fusion magnet, the LCP will allow attention to be turned to characterizing sources of AE other than conductor motions.

4) Results of experiments designed to advance our understanding of the mechanisms of elastic wave propagation in superconducting magnets are also included. This understanding is essential if AE signals are to be classified accurately.

5) Lastly, the conceptual development and early design of a new AE data recording and processing system will be presented. The system will be microprocessor-based and software-controlled.



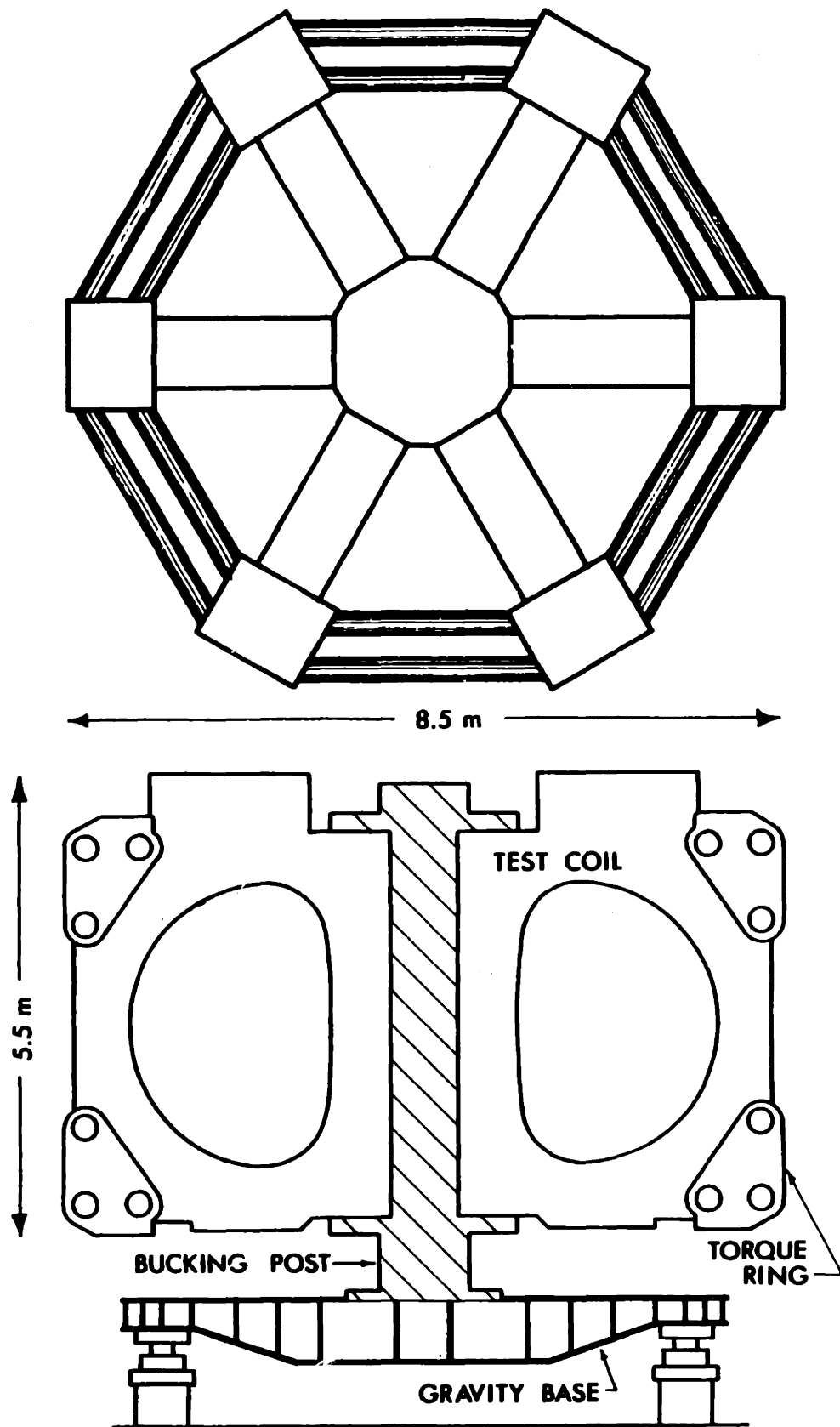


Fig. 3 Configuration of LCP magnets and their support structure.

## 2. AE INSTRUMENTATION SYSTEM

Figure 4 shows a schematic representation of the new AE instrumentation system; reference to this figure will be invaluable to understanding the discussion and data which follow.

### 2.1. Acoustic Emission Sensors

Piezoelectricity is the ability of certain materials to develop an electric charge or voltage potential proportional to a mechanical stress. Likewise, piezoelectric materials show the converse phenomenon — a strain proportional to an applied voltage.<sup>15</sup> Although there are many piezoelectric materials,<sup>15</sup> lead titanate zirconate has strong and stable piezoelectric effects and has become the most widely used piezoelectric ceramic.

Properties of the piezoelectric transducer which make it particularly suitable for AE applications include:

- (1) *Sensitivity.* Piezoelectric transducers are extremely sensitive in comparison to most other transducers, such as temperature, strain, and displacement gauges. As a result, disturbances can often be monitored at distant locations.
- (2) *Cost.* The transducer cost is moderate, making a system consisting of large arrays of sensors practical.
- (3) *Flexible frequency response.* Piezoelectric crystal geometry and transducer construction can be modified to produce a variety of transducer frequency responses. AE sensors fall into two general frequency response categories: 1) Resonant sensors: these are lightly-damped harmonic oscillators, with sharp resonances and high sensitivity only in their resonant regions, and 2) "Flat-type" sensors: these have smooth, broadband frequency responses. Resonant sensors are useful in applications where unwanted acoustic noise is present in frequency regions outside

---

<sup>15</sup>B. Jaffe, W.R. Cook Jr., and Hans Jaffe, Piezoelectric Ceramics, Academic Press, London (1971).

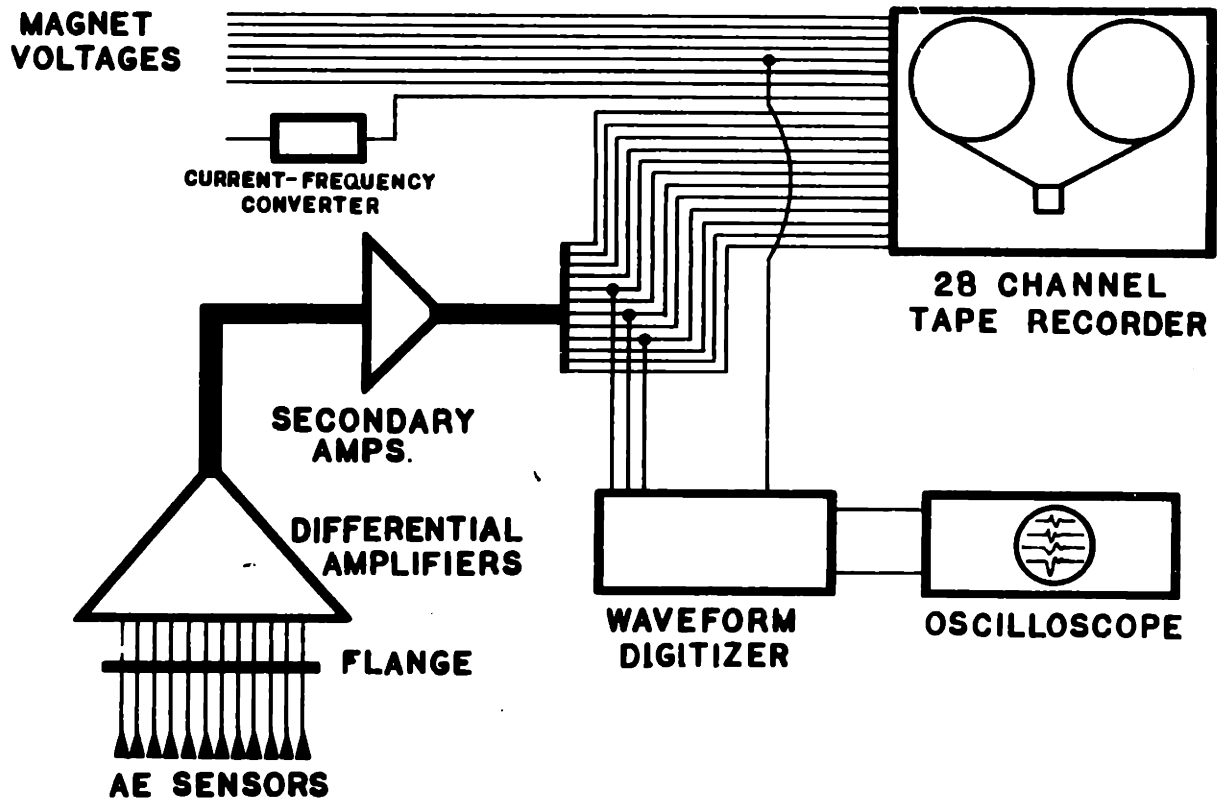


Fig. 4 Block diagram of AE data acquisition system.

the resonant band, or where detection of a disturbance can be ensured because of high sensitivity in the sensor's resonant region. Flat sensors are less sensitive than resonant types, but are excellent for applications where frequency analysis is desired.

- (A) *Resistance to thermal and mechanical shock.* Like most ceramics, piezoelectric crystals are rugged. A simple resonant-type sensor can be completed by designing and constructing a housing which electrically shields the crystal from interference, and physically shields its soldered connections. In addition, the ceramics are capable of withstanding great variations in temperature. As will be discussed later, AE sensors built for monitoring superconducting magnets must be particularly resistant to the effects of temperature and mechanical shock.

## **2.2. Unique AE Sensor Design**

The foundation of any acoustic emission instrumentation system is the AE sensor; approaches to sensor construction and design, however, vary widely according to the sensor's intended application. The cryogenic (low temperature) environment of the superconducting magnet poses some special problems for AE sensor design. In particular, because the magnets are cooled with liquid helium whose saturation temperature at atmospheric pressure is 4.2 K, the sensor must be capable of withstanding significant amounts of thermal stress. Conventional sensors usually cannot survive the thermal stress associated with this environment, but a specially-constructed sensor, developed and built at this laboratory, performs satisfactorily.

Although this AE sensor has worked adequately in the past, in some cases electrical noise interfered with the sensors' signals. (Piezoelectric crystals are inherently high impedance elements, and thus the transducer circuits are vulnerable to electromagnetic noise. Furthermore, cable lengths from the sensors to the outside of the magnet's cryostat (containment area) commonly run 25 m or more, making the circuits even more susceptible to noise.) Most notably, the circuits are vulnerable to noise generated by the magnets' power supplies, and a series of superimposed periodic spikes usually results, as remarked earlier. This problem made circuits capable of processing AE

signals in “real time” — or as they are played back from recordings — more complicated since the circuits had to distinguish and then discard the noise. Such a circuit was successfully designed for data from the MFTF magnet<sup>16</sup>; unfortunately, much of the circuit is specific to the MFTF data's noise, and cannot be used in general for other recordings made from other magnets.

A new sensor has been developed which is capable of electronically canceling the types of noise commonly affecting the circuits. This new sensor is a differential type; its design, construction, and characterization are presented below.

## **2.3. Differential Sensor**

### **2.3.1. Concept of the Differential Sensor**

Piezoelectric ceramic crystals are inherently polarized, having both a positive and a negative face; the differential AE sensor contains two piezoelectric elements, one oriented positively with respect to a ground and the other oriented negatively. In other words, one crystal is flipped over. Thus the differential sensor has two separate circuits with a common ground.

A differential amplifier has two inputs and one output; the output is simply the subtraction (and amplification) of the two inputs. The amplifier sees one input with a negatively-oriented signal, and one input with a positively-oriented signal, and the resulting output is a summation of the two input signals. The two input circuits have a common ground, so that electrical noise affecting one circuit will be nearly the same as the noise affecting the other. Because the differential amplifier sees nearly identical noise on each input circuit, the noise is nearly subtracted.

The noise on the two input circuits needs to be nearly identical, and to ensure this, the two piezoelectric elements' radii should not differ by more than a few percent. If they do, a significant difference in the crystals' impedances will result, causing the noise on the two circuits to differ and the difference to be amplified along with the desired signal.

---

<sup>16</sup>J. Lore, “Monitoring Disturbances in a Large Superconducting Magnet Using an Acoustic Emission Technique,” S.M. Thesis, Department of Mechanical Engineering, Massachusetts Institute of Technology, January 1983, (also see reference 12).

### **2.3.2. Construction of the Differential Sensor**

The differential sensor assembly is shown in Figure 5. A description of the sensor's construction and the dimensions of its various parts are contained in Appendix A.

The essence of the sensor's thermal shock resistance lies in the exclusive use of solder as a bonding material. (Piezoelectric crystals in commercial sensors are usually mounted with epoxy, which cracks at very low temperatures.) The copper jacket serves as both a physical and an electrical shield. The thin copper foil disk to which the piezoelectric crystals are soldered serves as a shock absorber needed because soldering directly to the more rigid brass shoe, despite the use of solder, results in the disk debonding from the shoe at very low temperatures.

### **2.4. Sensor Testing and Calibration**

Interpretation of AE data is dependent on accurate calibration of the AE sensors. Comprehensive calibration techniques should model the physical environment and excitation to which the sensor will likely be subject, a task aggravated in our case by the low temperature environment.

There are many procedures for calibrating AE sensors,<sup>17</sup> but they can be grouped into two general categories: absolute and relative calibration. Absolute calibration procedures yield the sensor's response in a frequency band to a known and quantified excitation. Relative calibration procedures yield sensitivity in a frequency range to an excitation which is repeatable but not quantified.

#### **2.4.1. Absolute Calibration**

Ideally, one would like to achieve the absolute calibration of AE sensors. In order to accomplish this, however, the typical excitation (or excitations) the sensor undergoes when mounted on the magnet must be identified and modeled. Superconducting magnets are extremely complex mechanical structures, often constructed in unusual geometries and consisting of many different materials, each with their own mechanical properties. Furthermore, our understanding of, and ability to characterize the mechanisms of stress wave emission in the magnets is limited. Hence theoretical prediction of the

<sup>17</sup>For a general discussion, see N.N. Hsu and F.R. Breckenridge, "Characterization and calibration of acoustic emission sensors," *Materials Evaluation*, **39**, 60 (1981).

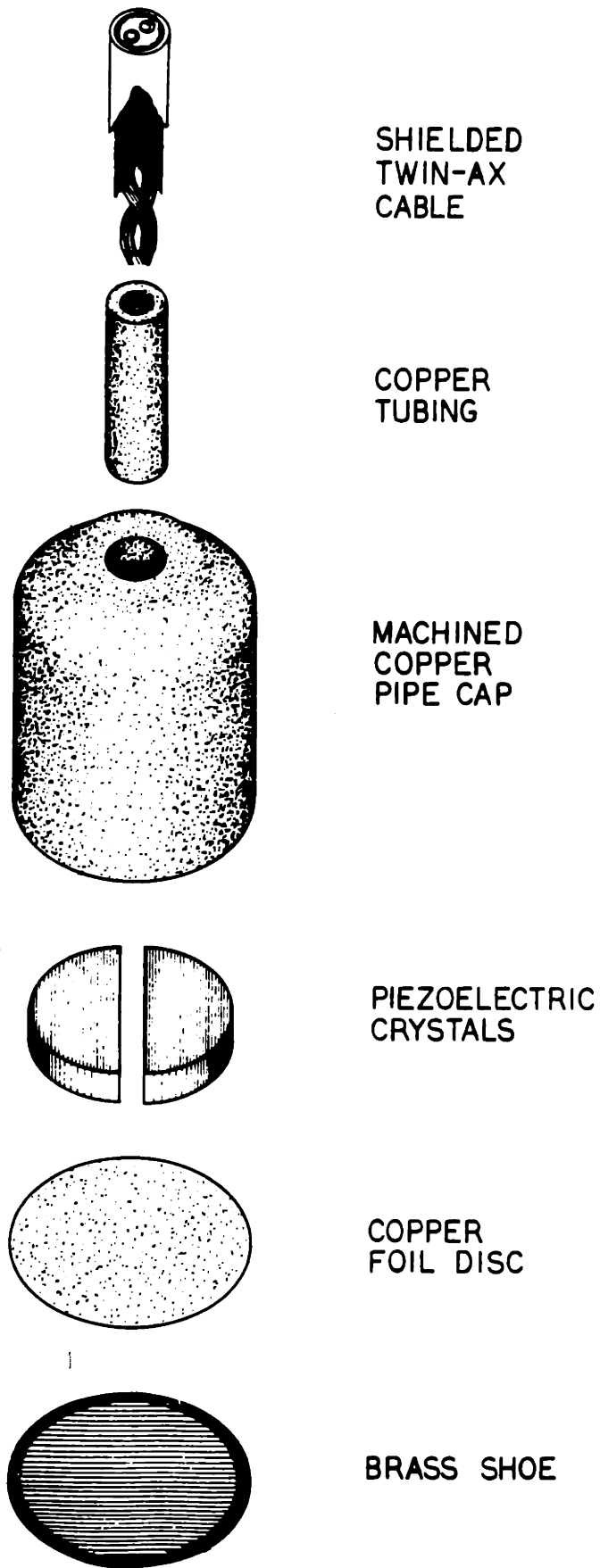


Fig. 5 Exploded view of differential sensor assembly.

excitation at a sensor's location due to a variety of mechanical disturbances originating in the magnet winding or structure is not feasible at this time, for it would require the understanding of both the initial disturbance and of the magnet's mechanical properties.

There are, however, absolute calibration procedures which are based on idealized excitations consisting of homogeneous wave fields, and as magnet dynamics become better understood, the results of these procedures may prove useful. One such procedure<sup>18</sup> uses an excitation and a propagating medium of sufficient simplicity to allow the theoretical prediction of the resulting stress wave field. An impulsive excitation (a pencil lead break for example) and a large block of some common material like aluminum or steel are typically used. Depending on the locations of the excitation and the sensor, a wave field consisting primarily of either compressional or Rayleigh surface waves can be produced. Although this procedure has been used with success, applying it to a 4.2-K environment would be extremely difficult because the propagating medium is a large metal block.

Another absolute calibration procedure<sup>19</sup> is based on the well-known principle of reciprocity for linear systems. Furthermore, the compactness of the propagating medium and the simplicity of the procedure make it potentially adaptable to the 4.2 K environment. Again, the stress wave field generated in this procedure can be composed predominantly either of Rayleigh surface waves, which arrive parallel to the surface of the receiving sensor, or compressional waves, which arrive normal to the sensor's surface. Because the composition of a typical stress wave field resulting from a typical AE event in a superconducting magnet has not been determined, the immediate benefits of such a calibration method are moot. However, as more information concerning stress wave propagation becomes available, absolute calibration of sensors for these two important wave types may become useful.

#### **2.4.2. Relative Calibration**

Relative calibration procedures are in general easier to conduct than absolute

---

<sup>18</sup>W.C. Leschek, "Acoustic emission transducer calibrator," *Materials Evaluation*, **33**, 41 (1975).

<sup>19</sup>H. Hatano and E. Mori, "Acoustic emission transducer and its absolute calibration," *J. Acoust. Soc. Am.*, **59**, 344 (1976).



methods, and often yield excellent information. These procedures are numerous,<sup>17</sup> each yielding different results; three have been used to characterize our sensors.

The face-to-face method is commonly used to calibrate commercial sensors. Figure 6 shows a block diagram of the procedure. Two sensors are clamped together, one acting as a driver and the other as a receiver. Variable frequency sinusoidal voltages are applied to the driver and the output of the receiving sensor is recorded. Because the response of the receiving sensor depends on the characteristics of the driving sensor, only relative calibration results; in addition, no attempt is made to match the wave field to which the sensor is likely to be subject in its application. Nevertheless, if the sensors are of the same design, regions of high sensitivity are revealed because the driver is efficient in the same frequency range in which the receiver is sensitive. Figure 7 shows a representative example of the face-to-face calibration procedure.

Another relative calibration method yields sensor response curves only in resonant regions. The loss of off-resonant response information is balanced, however, by the simplicity of the procedure. The AE sensor is driven with a variable frequency sinusoidal voltage. As the frequency approaches a resonant region, the impedance of the crystal drops, and hence the voltage across the crystal. Although it should be stressed that this procedure does not model the sensor's intended environment, the amount of voltage drop is in some sense a measure of sensitivity in resonant regions. Sensors built in this laboratory have been shown by this procedure to have similar responses in their resonant regions.

The third relative calibration procedure is even simpler. A block diagram is shown in Figure 8. Its purpose is to compare sensors' responses to a broadband, repeatable excitation. The sensor is mounted to a 1-m<sup>2</sup> by 1-cm thick stainless steel plate. A steel ball is dropped from a height of 2 cm and the response of the sensor is captured on a waveform digitizer.<sup>20</sup> Figure 9 shows a representative result of this procedure.

---

<sup>20</sup>An experiment was conducted to ensure that the sensor was receiving energy from the excitation in the frequency region of 1-40 kHz — the frequency response of the tape recorder used in the new instrumentation system.

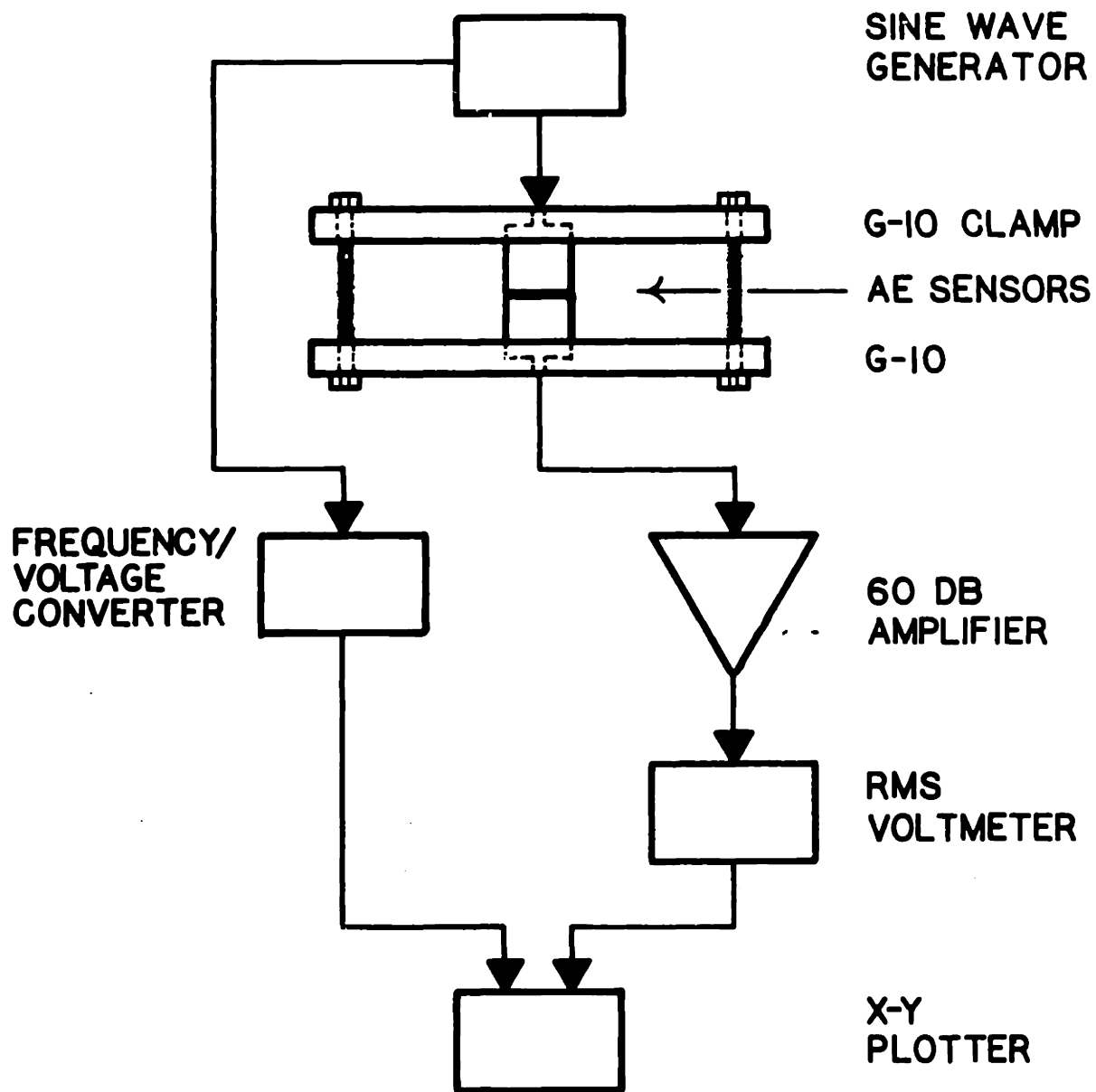
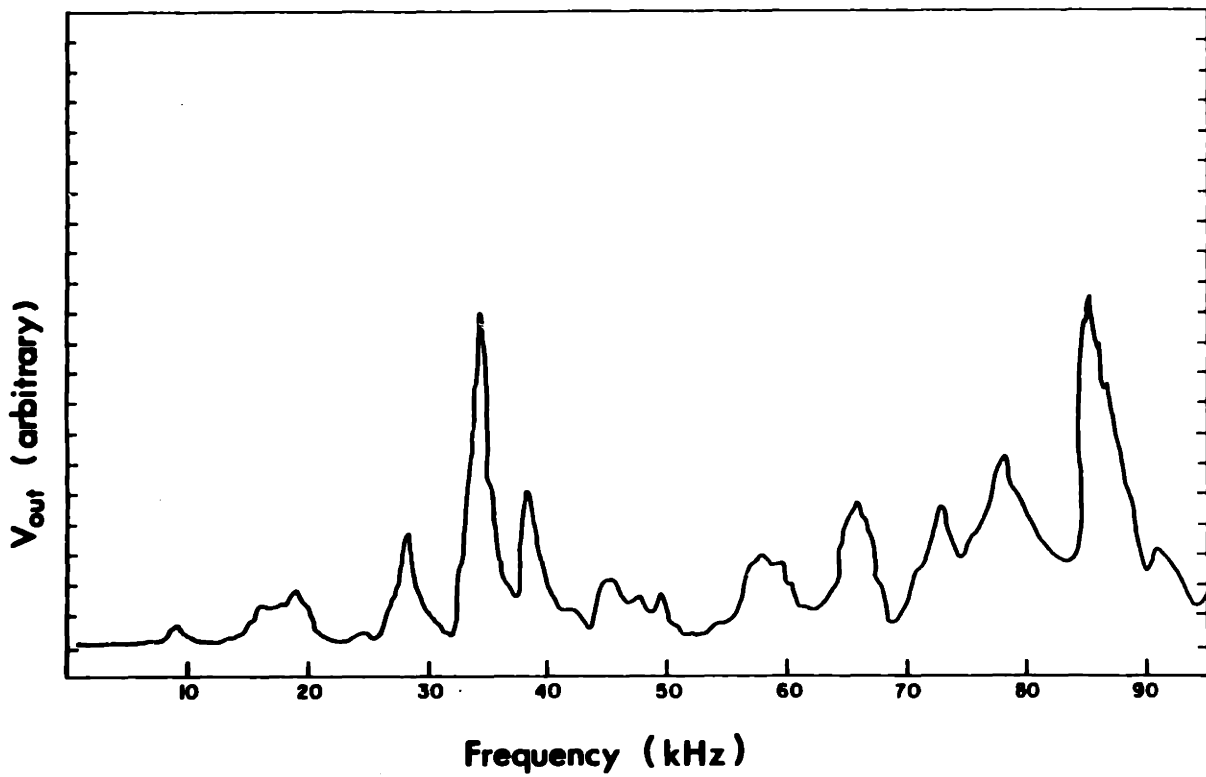


Fig. 6 Block diagram of face-to-face calibration procedure.



**Fig. 7** Representative result from face-to-face calibration procedure.

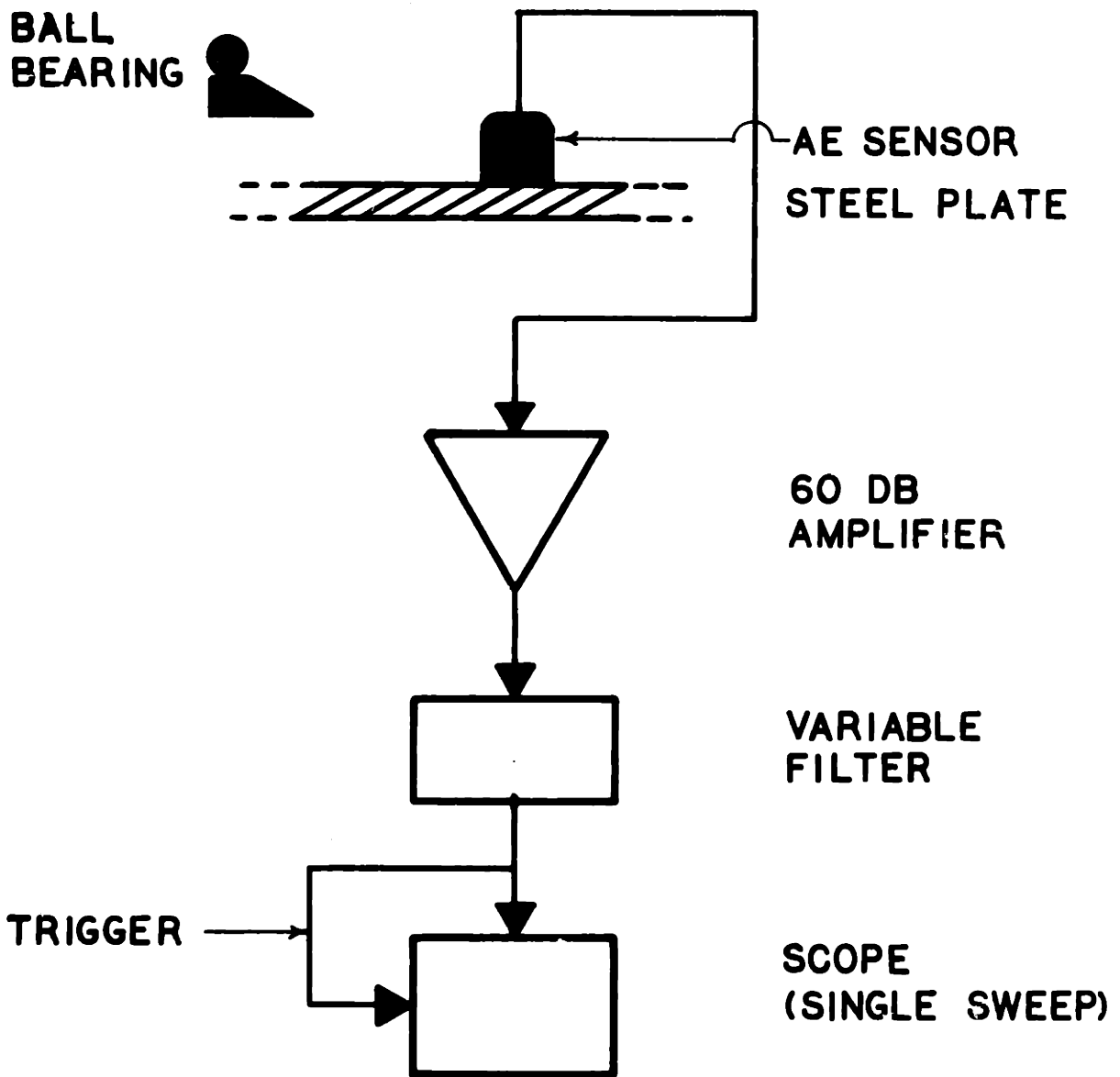


Fig. 8 Block diagram of broadband calibration procedure.

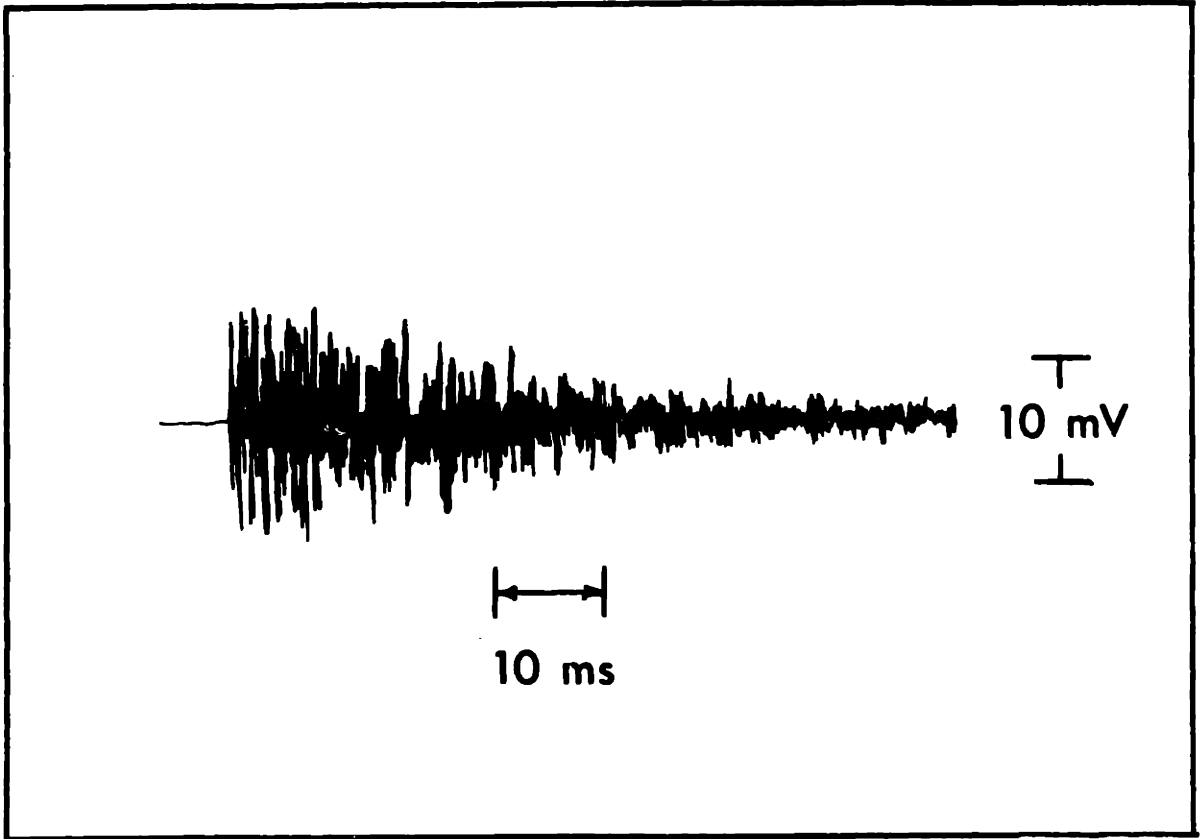


Fig. 9 Representative result from broadband calibration procedure.

## 2.5. Effects of Clamping

Acoustic emission sensors must be firmly attached to the structure they are to monitor; there is the need, therefore, for a reliable mounting apparatus and procedure. The necessary force can be applied in a variety of ways, but the most common is with spring force. (Spring mounting is particularly suitable in our application because the spring applies sufficient clamping force even when low temperatures would normally cause the sensor-structure coupling to loosen.)

An experiment was designed to test whether differing amounts of clamping force affected the sensitivity of the sensor. At the same time, the effect on sensitivity of a thin layer of vacuum grease was determined, since it is widely believed that such a layer ensures good sensitivity.<sup>21</sup>

The experimental setup is essentially the same as that for the face-to-face calibration procedure (see Figure 6) with the exception that a smooth copper bar (2 cm x 1 cm x 10 cm) is placed between the sensors in order to isolate the clamping force solely on the receiving sensor; the apparatus ensures that the driving sensor's clamping force does not change while the receiving sensor's clamping force can be varied. The experiment was repeated at both room temperature and 4.2 K, for three representative clamping forces,<sup>22</sup> and each time with and without vacuum grease. The results are characterized by those in Figure 10. To summarize the results:

- (1) Within the wide range used, clamping force is not an important factor in sensor sensitivity. Therefore, only moderate clamping force is necessary to ensure good sensitivity.
- (2) With moderate clamping, vacuum grease has no distinguishable effect on sensitivity in the frequency range of 1-300 kHz.

Secondary, but nonetheless important additional conclusions can be drawn from the results:

<sup>21</sup>Companies specializing in acoustic emission equipment, for example, sell "special" vacuum grease for mounting their sensors.

<sup>22</sup>The three clamping forces have not been quantified, but are characterized only as light, moderate, and heavy clamping: lightly clamped sensors could be moved with ease with the hand, while heavily clamped sensors could not. The three forces were repeatable, however, by measuring the distance between the two clamping bars.

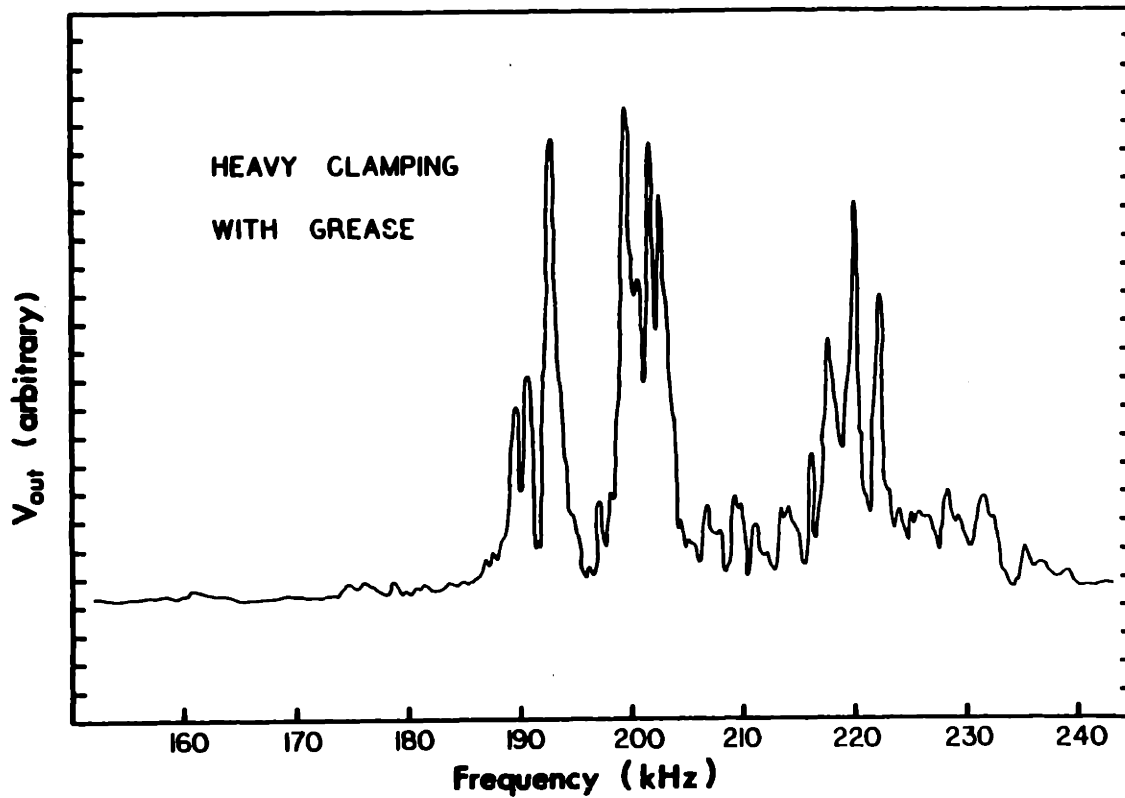
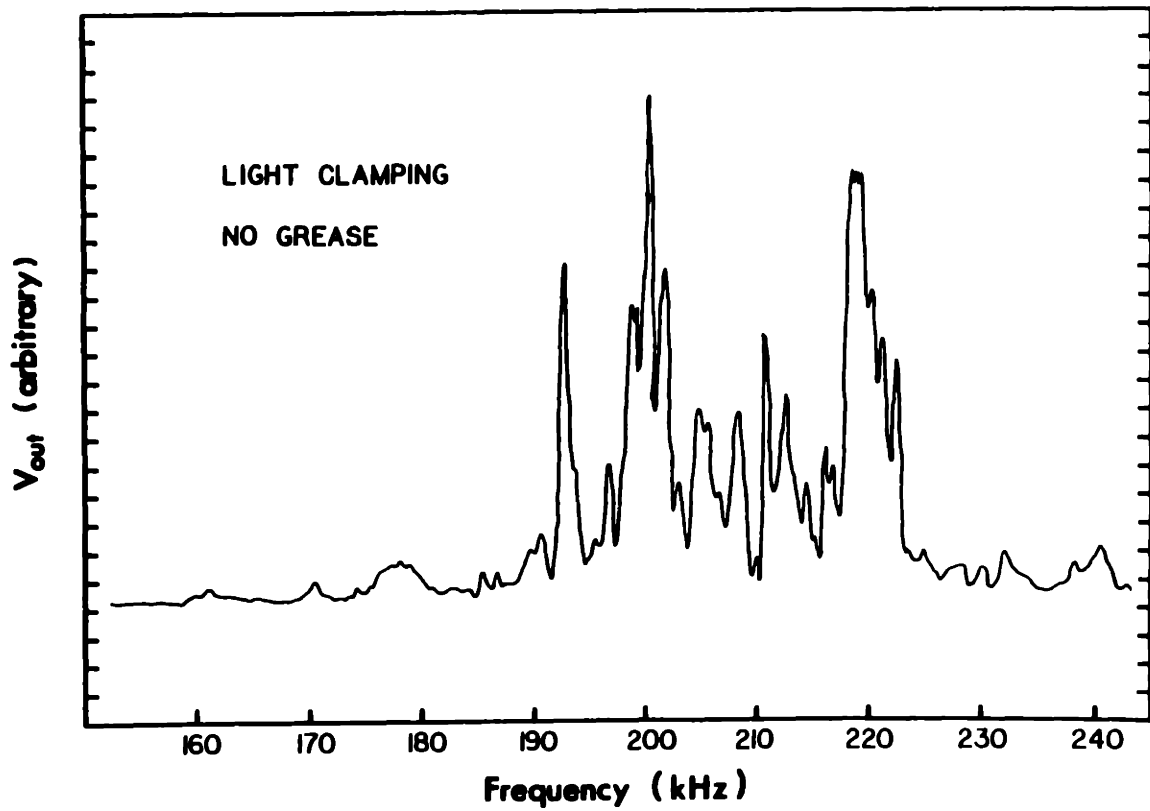


Fig. 10 AE Sensor frequency response with light clamping and no vacuum grease (top) and with heavy clamping and grease (bottom).

- (1) The detailed frequency response curves change drastically when the clamping force is changed or when the sensor is unclamped and then re-clamped with the same force. In other words, the response curves are not reproducible by any known means. To further demonstrate this, a particular resonant frequency of the driver/receiver pair was chosen and fixed, and the clamping force varied over time. Figure 11 shows that the amplitude of the receiving sensor changes radically with varying clamping force. It can be inferred that unrepeatable changes in the coupling of the sensor to the copper bar are occurring. The implication of this result is that the benefits of a detailed calibration of the sensors are questionable, since it is unlikely that the same response curve could ever be made reproducible.
- (2) Fortunately, the results also show that the frequency regions of sensitivity *do not* change significantly with either varying clamping force or the presence of vacuum grease. Thus sensors can be compared by their regions, or envelopes, of sensitivity. (This conclusion was supported by results of broadband calibration, which showed that when a sensor was mounted, detached, and remounted with moderate clamping force, its broadband sensitivity did not change significantly.)

In conclusion, our AE sensors can be mounted simply and quickly since broadband sensitivity is not affected by different clamping forces or the presence of vacuum grease. The detailed response curves cannot be made constant because of unrepeatable changes in the coupling of the sensor to the structure; cruder calibration, however, is possible since sensitivity envelopes are not affected by clamping force or the presence of vacuum grease.

## **2.6. Effects of Mylar**

Proper sensor circuit grounding is an effective means of controlling noise. In general, the circuit should be grounded at only one point since even small electric potential differences between multiple grounds generate unwanted currents which result in noise.



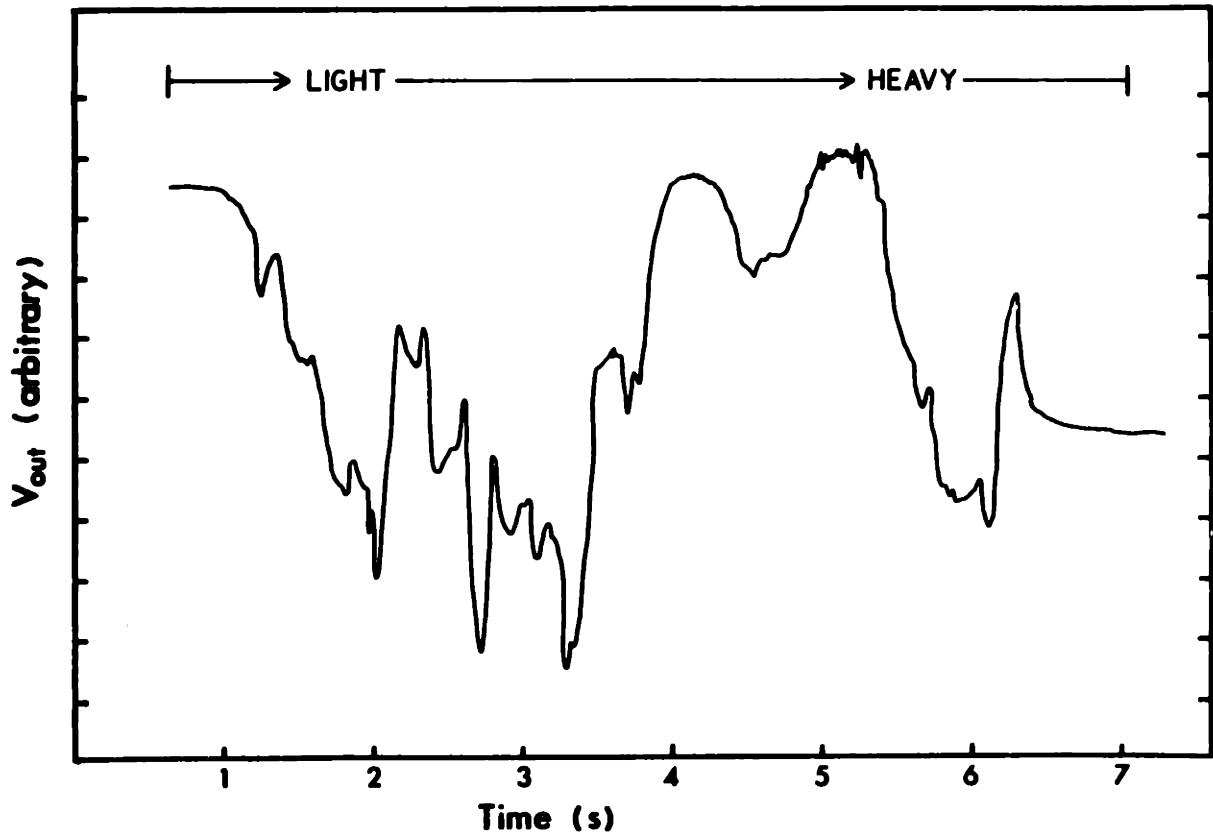


Fig. 11 Sensor response at a fixed frequency of 200 kHz to a continuously changing clamping force.

In some cases the noise induced in this manner is of the same order of magnitude as weak AE signals.

For logistical reasons,<sup>23</sup> it is convenient to ground the AE instrumentation system at the preamplifier stage (refer to Figure 4); thus it becomes necessary to unground the sensor relative to the magnet casing.<sup>24</sup> A material for this purpose must be electrically nonconducting but acoustically transparent.

Mylar tape is often used in cryogenic applications because of its insulating qualities and its durability at extremely low temperatures. It is available in a variety of thicknesses. For these reasons, Mylar tape was a candidate for the purpose of electrically isolating the sensor from the magnet.

An experiment was conducted to determine the effect of a layer of 0.2-mm Mylar tape on sensor response. The experimental setup is exactly the same as that for the face-to-face calibration except for the presence of Mylar between the driver and the receiver. The results can be summarized as follows: at room temperature, the Mylar causes about a 20 % decrease in the sensitivity of the sensor, but at cryogenic temperatures — in this case the boiling point of nitrogen (77 K) — there is no loss of sensitivity.

It can be concluded, therefore, that Mylar can be used to electrically isolate the sensor from the magnet while remaining acoustically transparent as long as it is used at cryogenic temperatures. (One possible explanation for the difference of effects at room and cryogenic temperatures is the fact that the adhesive on the tape as well as the tape itself becomes brittle at low temperature and becomes acoustically transparent.)

## 2.7. Effects of Temperature

An examination of AE data from the MFTF-B magnet<sup>12</sup> reveals that three of the twelve sensors were weak or inactive. It is unlikely that the sensors were simply on particularly quiet regions of the magnet, since sensors mounted in other symmetric positions showed normal AE activity. Furthermore, ambient noise on the

<sup>23</sup>The commercial preamplifiers would have to be modified in order to isolate the common ground of their power supply and the sensor circuit.

<sup>24</sup>The sensor casing (see Figure 5) is part of the sensor's electrical shield, and hence must be isolated from the magnet casing.

weak sensor circuits was also much lower than active sensor circuits making more likely the possibility that the sensors had failed or their coupling to the magnet had deteriorated. A crude calibration procedure which had been performed at room temperature showed that all of the sensors were relatively sensitive, indicating that the loss of sensitivity occurred during or after cooldown. Unfortunately, the sensors were not similarly calibrated following the test, making it impossible to know whether the loss of sensitivity was a temporary or permanent effect.

In another case,<sup>25</sup> the sudden loss of sensitivity of an AE sensor during an experiment conducted at 4.2 K was observed. After warming the sensor to room temperature, however, it showed normal sensitivity. The experiment was repeated several times, and on one occasion the effect reoccurred; unfortunately, it could not be deliberately repeated by any means attempted.

Because of these observations, a control experiment was designed to attempt to isolate the cause or causes of the sensitivity loss. Four AE sensors were mounted side-by-side to a copper block. Firmly attached to the block was a copper rod which ran through the top of an experimental dewar to the ambient laboratory environment. The sensors/copper block assembly was precooled in a bath of liquid nitrogen, and then lowered into a bath of liquid helium. At regular intervals, the copper rod was excited with a spring-loaded center punch which delivered a broadband excitation to the sensors, and their responses were captured on a waveform digitizer and output to an X-Y plotter. Data was taken at one hour intervals for four hours, and on two separate occasions. No significant loss of sensitivity was detectable in any of the four sensors tested.

In one sense, the results were discouraging, since it would be informative to know the causes of the apparent effect in order to avoid them or modify the sensors to overcome them. The first sensors installed on the GD-LCP coil will be monitored for these effects.

---

<sup>25</sup>This occurred during an experiment conducted in this laboratory and is documented.

## 2.8. Differential Amplifier

The differential amplifier provides the first stage of amplification for the AE sensor circuits (see Figure 4). Desirable specifications include:

- (1) *Common-mode noise rejection.* The degree to which common mode noise is rejected by the differential amplifier is one of its basic specifications. Approximately 60 dB of noise rejection in the bandwidth of our tape recorder (1-40 kHz) would be desirable.
- (2) *Frequency response.* The frequency response ideally should be flat from about 1 kHz — in order to discard 60-Hz noise — to about 500 kHz, the upper frequency limit of our laboratory instruments.
- (3) *Gain.* Unamplified AE event peak amplitudes range from approximately 0.1 to 1 mV. It is desirable to have the inputs to most laboratory equipment (including the equipment used for AE signal processing) range from 1 to 10 V peak. An overall gain of the sensor's output should therefore be approximately 10,000 or 80 dB. In addition, in a two-stage amplification system it is desirable to have more gain at the first stage so that noise entering the circuit after the first stage will not have as great an affect on the circuit's signal-to-noise ratio. For these reasons, a gain of 1000, or 60 dB was chosen for the preamplifier.
- (4) *Signal-to-noise ratio.* In order to avoid having noise mask weak AE events, the preamplifier should have a low ambient noise level. A noise level of 1  $\mu$ V, which is about 40 dB less than a weak AE signal, would be considered excellent.

A commercial amplifier<sup>26</sup> which met these requirements was chosen. The preamplifier has excellent common-mode noise rejection of 60 dB over its *entire* frequency range (2-600 kHz), is gain-switchable from 40 to 60 dB and has an operating noise level of 2  $\mu$ V.

---

<sup>26</sup>The Physical Acoustics model 1220C.

## **2.9. Secondary Amplifier**

The purpose of the secondary amplifier is to provide up to 20 dB of additional gain in the sensor circuits. Although the amplifier used in past monitoring systems performed adequately, its frequency response was too narrow for the signal processing and analysis planned and its gain was unpredictably subject to temperature changes. Desirable specifications include:

- (1) The bandwidth of the amplifier should coincide roughly with that of the preamplifier, so as not to filter unnecessarily potentially useful information.
- (2) The gain should be continuously variable in order to allow each sensor circuit to be gain-adjusted to roughly the same overall sensitivity, (see section 3.7.).
- (3) Its dynamic range should be compatible with the signals from the preamplifier; in other words, the secondary amplifier should not be overloaded by a strong signal from the preamplifier, and its operating noise level should not mask a weak signal from the preamplifier.
- (4) The secondary amplifier should have an input impedance compatible with the output of the preamplifier and an output impedance compatible with the input impedance of the tape recorder.

Although commercial amplifiers satisfying these requirements exist, it was decided that the simplicity of the device warranted in-house design and construction. A 24-channel version of this amplifier has been built for use on the Large Coil Program. Its specifications include: 1) frequency response of 10-100,000 Hz  $\pm$ 1 dB; 2) gain continuously variable to 32 dB; 3) low input and output impedance; and 4) peak input voltage before clipping of 0.6 V. (Appendix B contains the circuit diagram of the amplifier.)

## **2.10. 28-channel Tape Recorder**

A 28-channel, multi-speed tape recorder<sup>27</sup> is used to record simultaneously signals

---

<sup>27</sup>The Honeywell 5600E.

from AE sensors, voltage taps from the magnet, voltages corresponding to the magnet current,<sup>28</sup> and the tape operator's voice. The tape recorder has the following specifications:

- (1) *Frequency response.* Tapes can be recorded at either 7.5 or 15 inches per second (IPS), and the frequency response of the recorder differs for each speed. The recorder is essentially flat (within 3 dB) from 1-40 kHz at 7.5 IPS and from 1-50 kHz at 15 IPS.
- (2) *Dynamic range.* The ambient noise level of the recorder is 175 mV and the maximum input that will be recorded (in the recorder's frequency response range) without distortion is 8 V, making the dynamic range 33 dB.
- (3) *Inter-channel synchronization.* The alignment of the recording and playback heads determines the degree of synchronization between the channels. The margin of error in aligning the heads is 10  $\mu$ s at 7.5 IPS and 5  $\mu$ s at 15 IPS. In addition, due to the division of the twenty eight tracks on two head blocks, time differences of 65  $\mu$ s exist between odd and even numbered tracks. This time difference must be taken into account when time differences of AE events on odd and even tracks are being determined.

## 2.11. Waveform Digitizer

It is important for the operator of the acoustic emission system to monitor data acquisition in real time, and for this purpose a waveform digitizer is used. The operator can observe either independently or simultaneously data being sent to or recorded on four channels of the tape machine, thus partially verifying the proper operation of the system.

---

<sup>28</sup>Voltage taps are available for each of the fourteen coil layers. In addition, a tap will be provided for: terminal voltage; layers 1-7; and layers 8-14. Both voltage tap and current shunt signals will be 0-10 V.

## **2.12. Sensor Guards**

It is sometimes necessary for AE sensors to remain mounted on magnet systems for long periods of time, during which the performance of magnet maintenance work can damage the sensors. Therefore, sturdy diecast aluminum boxes, (9 cm x 4 cm x 3 cm) have been modified to house the differential sensor and its twin-axial connector. Use of such a guard box will result in a longer operating lifetime for each sensor.

### 3. LARGE COIL PROGRAM DATA ACQUISITION

#### 3.1. Large Coil Program (LCP)

One of the major projects sponsored by the United States Department of Energy Office of Fusion Energy (DOE-OFE) is the development of superconducting magnets for fusion reactors. Central to this effort is the Large Coil Program (LCP),<sup>29</sup> which was established in order to provide the technology necessary to build the superconducting magnets for tokamak fusion reactors.

The stated key objective of the Large Coil Program is, "to develop a magnet technology base sufficient for commitment to a superconducting tokamak reactor through the design, construction, testing, evaluation and comparison of different large toroidal field coils that operate reliably at a peak field of 8 tesla and other conditions typical of a tokamak reactor magnet."<sup>29</sup> In other words, the LCP was designed to test several possible design solutions of fusion-scale superconducting magnets for full scale tokamak reactors. The panel which conceived the LCP recommended that the coils be designed and built by industry rather than national laboratories.

The specifications for the LCP were completed late in 1976 and were based on the philosophy that the test coils be a reasonable fraction of the coil size envisioned for tokamak reactors. The specifications include performance and dimensional requirements, (bore size and peak field for example), but intentionally allow a great deal of freedom in the internal design of the winding.

Three domestic proposals from industrial teams were eventually accepted: General Dynamics/Convair Division, General Electric, and Westinghouse. In addition, there are three international participants: EURATOM, Japan, and Switzerland. Each design concept is different, most notably in the areas of conductor design, conductor operating current, winding and conductor configuration, and structural material and configuration. All six of the magnets are expected to be tested in 1985.

---

<sup>29</sup>P.N. Haubenreich, J.N. Luton and P.B. Thomson, "The role of the large coil program in the development of superconducting magnets for fusion reactors," *IEEE Trans. Magn.*, MAG-15, 520 (1979).



### **3.2. Large Coil Test Facility**

When the Large Coil Test Facility, located at the Oak Ridge National Laboratory, is fully operational, it will consist of six test coils, a support structure for the coils, small magnets used to pulse individual test coils, a large vacuum tank which will provide thermal insulation for the coils, and various other facility support elements, such as instrumentation rooms and data acquisition systems.

The support structure for the test coils is composed of a central column, called the bucking-post, which is continuous with a gravity base and two torque rings that clamp the outer corners of the test coils. The torque rings are continuous, allowing the testing of less than the full capacity of six coils without modification or the need for dummy coils. In addition, the facility is designed to accommodate larger and heavier coils in the future. Refer to Figure 3 for a plan and elevation of the magnets and their structural support system.

### **3.3. General Dynamics LCP Coil**

Although it was first intended to install and test all six LCP magnets at once, delays in several of the manufacturers' schedules have resulted in the decision to conduct a preliminary test on two coils, the U.S. coil built by General Dynamics (GD), and the Japanese coil, both of which have been installed at the test site. The GD coil was chosen for our acoustic emission studies while the Japanese coil is to be monitored independently by the Japanese. Some of the more important features of the GD coil are discussed in Appendix C.

### **3.4. AE Program Objectives**

The LCP offers a unique opportunity to study AE data and relate them to the performance of the magnets, both in the long and short term. One of the primary objectives of this work has been to develop techniques which will enable future investigators to interpret AE data. This work has focused on two such techniques: (1) the determination and classification of disturbances resulting in acoustic emission through the analysis of AE signals and (2) increase our ability to localize the origin of AE events.

### **3.4.1. Classification of AE Events**

The LCP coils are designed to be extremely stable, and hence the likelihood of a magnet quench due to disturbances such as conductor motion is small. Conductor motion events are still expected to occur, however, and will be recorded, but attention will also be given to characterizing non-conductor-motion events.

The identification and classification of strain-induced structural AE events is necessary if AE is to be used to help ensure the structural integrity of superconducting magnets. It is assumed that the type of structural-motion events that are relevant to the safety and reliability of the magnet systems are strain-induced. Because of the size and complexity of the LCP magnets and their support structure, it is probable that these strain-induced structural AE events will originate from a variety of sources, possible among which are: (1) the magnet support structure, (2) the magnet casing, and (3) the magnet winding. (The section on sensor configuration describes the choice of sensor locations in order to identify the AE events originating in these regions.)

### **3.4.2. Event Localization**

In most cases, the origin of an AE event is assumed to be in the neighborhood of the sensor first detecting it. A more accurate determination of the origin of the disturbance could be made by combining information gathered by a number of sensors located strategically around the source with a knowledge of stress wave behavior in the magnet. This is the basis of triangulation techniques, which have been used on structures of relatively simple geometry. Although it has been emphasized that superconducting magnet systems are complex mechanical structures, a general understanding of stress wave behavior in the magnets may lead to the use of a triangulation technique which results in a significant improvement over the one-sensor technique.

In addition, new information regarding the attenuation of high frequency components of AE signals originating from within the coil winding (to be presented below) may be used to distinguish these signals from those originating from outside the winding. More generally, it may be possible to apply more sophisticated techniques which recognize differences in the spectra of AE events as an indication of their origin.

### **3.5. Sensor Installation**

Because the Large Coil Program will be operated for a long period of time, a method of sensor installation and maintenance was developed to help ensure sensor reliability. One consideration is the protection of the AE sensor from the physical abuse that is inevitable in an ongoing project of this scale. Another is that the mounting method must be capable of compensating for the changes in the sensor coupling due to wide temperature changes.

A sensor mounting apparatus developed to meet these requirements is shown in Figure 12. The two stainless steel studs are welded to the magnet casing. The Belleville washers act as stiff springs so that the sensor guard box does not loosen when the magnet casing contracts due to cooldown. The G-10 strip applies a spring force to clamp the sensor firmly to the magnet surface.

The result is a sensor assembly which has the following important features: (1) it is simple to mount, (2), it protects the active transducer from most physical abuse, and (3) it remains effective in clamping the sensor to the magnet even when subject to extreme temperature changes.

Cables running from the feedthroughs located on the side of the cryostat to the sensors are strain relieved every 75 cm to minimize the possibility of connections being weakened or broken.

### **3.6. Sensor Locations**

Positions of AE sensors to be mounted on the GD coil are shown in Figure 13. (Their coordinates are listed in Appendix D.) They can be broken into the following groups:

- (1) **Sensors 1-4** are intended to be the first to respond to AE events originating in the upper and lower torque rings.
- (2) **Sensors 5-8, 20, and 21** will be the first to respond to signals originating in the bucking post.

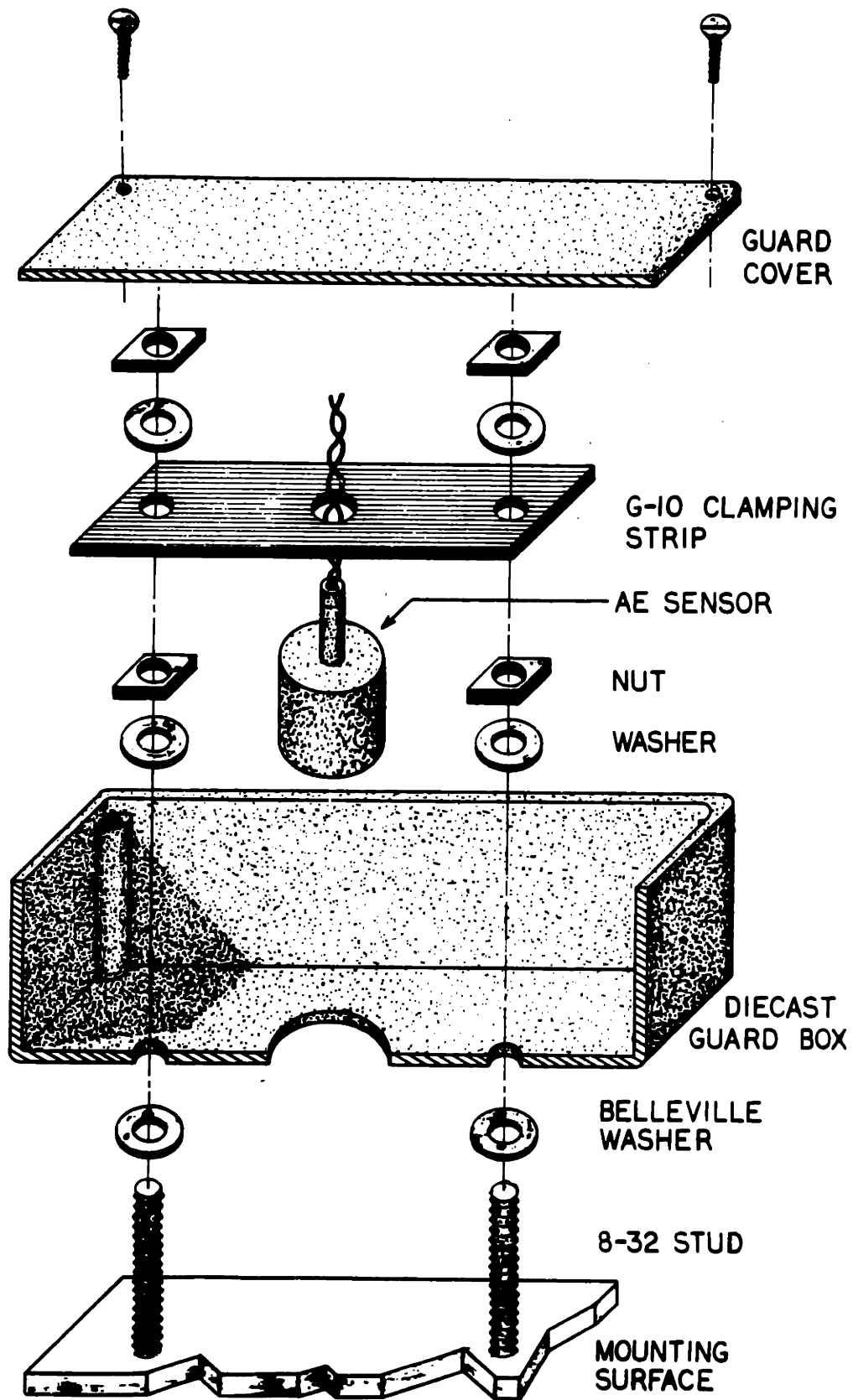


Fig. 12 Sensor mounting apparatus for LCP sensors.

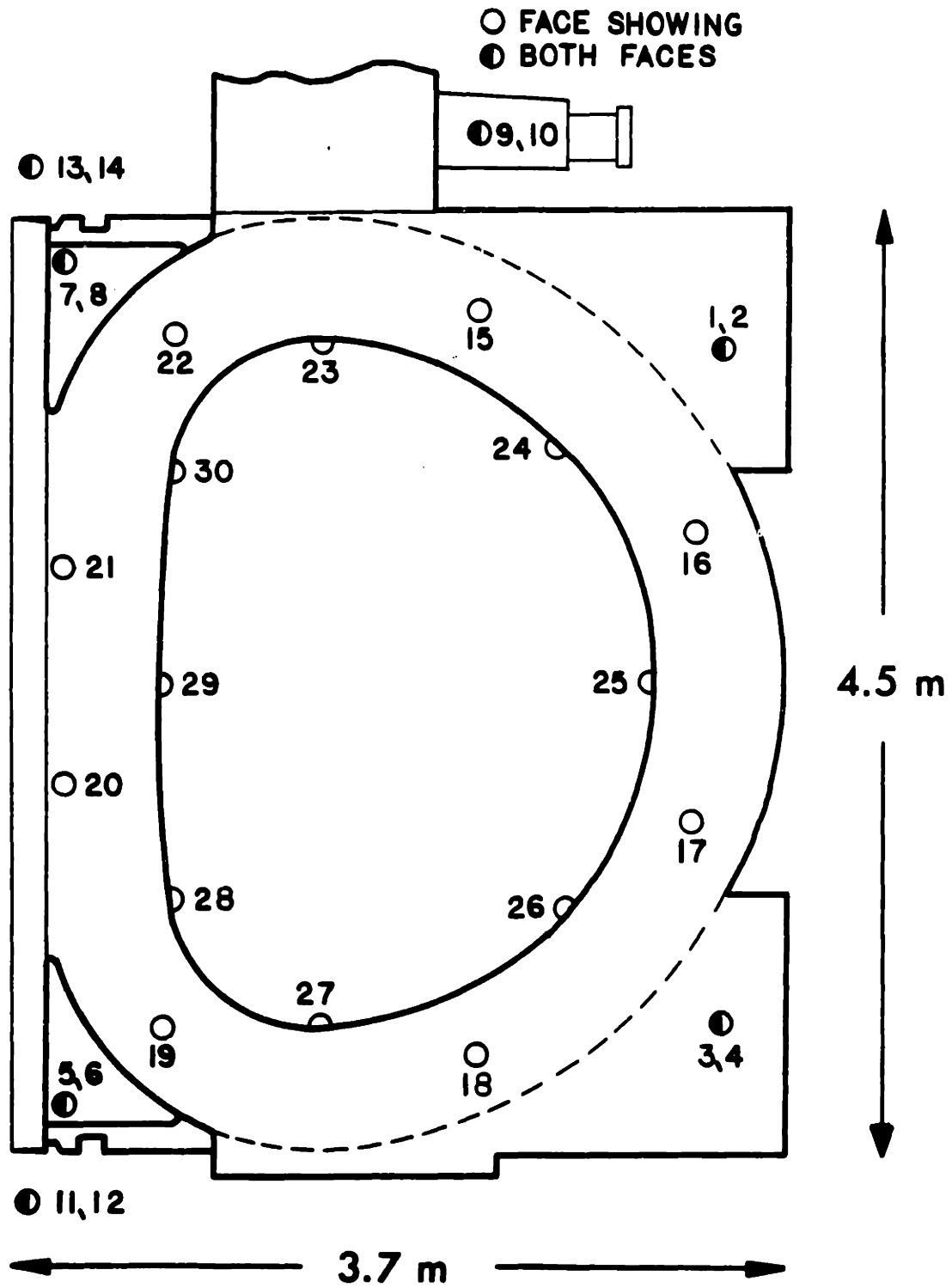


Fig. 13 Sensor locations for GD-LCP coil. Sensor pairs that are marked "both sides" have the odd numbered sensor on the opposite face, and the even numbered sensor on the face showing.

- (3) **Sensors 9 and 10** are located close to the entrance and emergence of the high-current leads and will sense disturbances originating in the current leads.
- (4) **Sensors 11-14** are located on the four spanning spokes straddling the GD coil.
- (5) **Sensors 15-30** will be the first to respond to signals coming from the coil winding and casing, including conductor-motion events.

Although only twenty-four channels are reserved for AE sensor signals on the tape recorder, thirty sensors have been mounted on the GD coil for two reasons: (1) in every case in the past, at least some of the sensors were inoperative in the 4.2 K environment, hence some redundancy in sensors should ensure twenty-four working sensors, and (2) should more than twenty four sensors work after cooldown, the configuration chosen allows some flexibility in sets of sensors to be recorded.

### **3.7. System Calibration**

Accurate calibration of the AE instrumentation system installed on the GD magnet is essential if meaningful interpretations of AE data are to be made. Unfortunately, calibration performed at 4.2 K must be remotely operated. Because more time is necessary to develop a calibration procedure which can be performed in the cryogenic environment, a room temperature calibration procedure was developed for the GD coil. An outline of the procedure follows:

#### **3.7.1. Phase One**

Forty differential AE sensors were built and fitted into guard boxes. Each sensor/guard box pair was then calibrated using the broadband excitation procedure (see section 2.4.2.). With the exception of two sensors with very weak outputs, suggesting some important defect, the peak-to-peak responses were always within 10 % of one another.

#### **3.7.2. Phase Two**

A modified<sup>30</sup> spring-loaded center punch was used to deliver a repeatable broadband excitation to the magnet casing.

<sup>30</sup>The punch is modified only in that its sharp point is removed.

Each operable<sup>31</sup> sensor was then excited with the center punch at a distance of  $\approx 5$  cm from its center. The stress waves resulting from the impact propagated to other sensors mounted on the magnet. The preamplified signals from the primary sensor and other (secondary) sensors responding were recorded on the multichannel tape recorder.

### 3.8. GD System Calibration Results

#### 3.8.1. Sensor Response

The results of laboratory broadband calibration of the thirty sensors mounted on the GD coil showed that their sensitivities were nearly identical. When mounted on the GD coil, however, their responses differ significantly. Figure 14 shows the responses of two of the thirty sensors before and after mounting. Obviously, meaningful interpretation of AE data must be based on the results of broadband calibration with the sensors mounted on the magnet.

Table 1 presents GD calibration data for each sensor: peak amplitude, energy content parameter,  $E_0$ , and signal duration parameter,  $T_b$ , are included. (The definitions and methods used to compute  $E_0$  and  $T_b$  are presented in Sec. 3.8.3.) From the data it may be concluded:

- (1)  $E_0$  values can differ by a factor of 30 while their peak amplitudes may differ only by a factor of two, (sensors 9 and 16).
- (2) Sensors mounted in similar locations on the magnet show similar responses. Sensor 1-4, mounted on the upper and lower torque rings, for example, all show relatively high energy content and long signal duration times. In contrast, sensors 15-23, mounted on the coil face, all show relatively low energy content and short duration times (with the possible exception of sensor 23).

---

<sup>31</sup>Because of delays in coil installation, sensors 11-14, to be mounted on the restraining rods, were not mounted at the time of the calibration test.

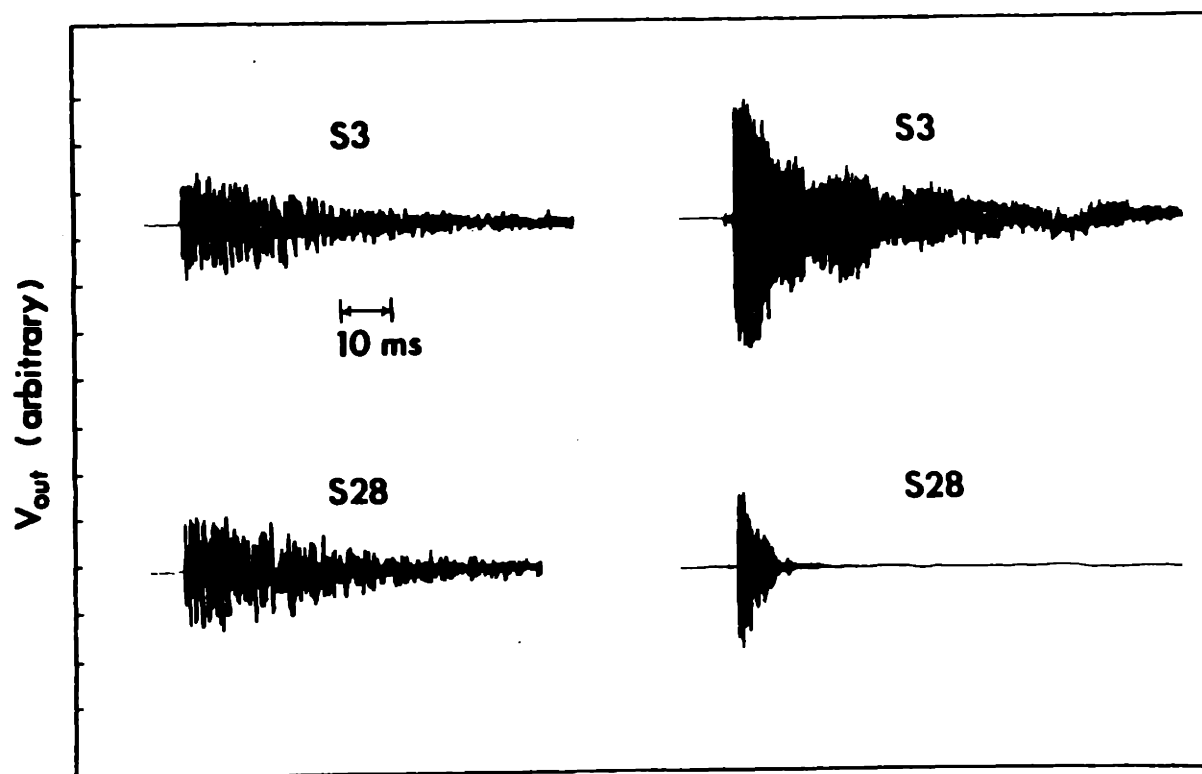


Fig. 14 Calibration response of two sensors before and after mounting on the GD coil.



**Table 1: GD Sensor Response**

| <u>Sensor (#)</u> | <u>Peak* (V)</u> | <u>E<sub>0</sub> (arb.)</u> | <u>T<sub>b</sub> (ms)</u> |
|-------------------|------------------|-----------------------------|---------------------------|
| 1                 | 9.6              | 29.0                        | 34.7                      |
| 2                 | 5.6              | 20.6                        | 27.4                      |
| 3                 | 9.1              | 31.8                        | 34.4                      |
| 4                 | 8.6              | 18.9                        | 16.7                      |
| 5                 | 8.0              | 6.5                         | 8.1                       |
| 6                 | 7.3              | 4.0                         | 5.8                       |
| 7                 | 8.9              | 18.9                        | 5.3                       |
| 8                 | 7.9              | 9.8                         | 6.3                       |
| 9                 | 10.4             | 60.8                        | 19.3                      |
| 10                | 9.2              | 26.4                        | 16.8                      |
| 11-14             | NA†              | NA                          | NA                        |
| 15                | 1.9              | 0.32                        | 5.5                       |
| 16                | 6.3              | 2.2                         | 6.3                       |
| 17                | NA               | NA                          | NA                        |
| 18                | 8.1              | 8.2                         | 4.1                       |
| 19                | 6.6              | 5.0                         | 3.5                       |
| 20                | 8.0              | 6.4                         | 3.4                       |
| 21                | 6.5              | 1.9                         | 2.6                       |
| 22                | 8.5              | 2.6                         | 9.1                       |
| 23                | 9.0              | 11.8                        | 12.3                      |
| 24                | 7.1              | 3.8                         | 3.7                       |
| 25                | 9.6              | 27.3                        | 9.0                       |
| 26                | 9.7              | 3.6                         | 11.7                      |
| 27                | 5.0              | 2.7                         | 5.6                       |
| 28                | 9.7              | 3.6                         | 5.5                       |
| 29                | 9.0              | 7.7                         | 7.1                       |
| 30                | 7.8              | 9.4                         | 8.0                       |

\* After an amplification of 60 dB.

† Sensors were not mounted at the time of calibration.

### 3.8.2. Wave Speed

Various types of stress waves can exist in elastic solids.<sup>32</sup> Only two can exist in an infinite medium: compressional waves (also known as dilatational, longitudinal, or pressure waves) and shear waves (also known as distortional, rotational, or equivoluminal waves). In a semi-infinite medium, however, a third type of wave, of special importance to acoustic emission applications, can exist: Lamb waves<sup>32</sup> exist only on and near a semi-infinite medium's traction-free surface. Of an infinite number of Lamb wave modes, Rayleigh surface waves are the lowest and are usually of the greatest practical importance; for example, the destructive force of a large seismic disturbance (earthquake) is due to Rayleigh surface waves. It has also been shown that Rayleigh surface waves can dominate compression and shear waves at the surface of a thick infinite plate.<sup>19</sup>

The propagation speed (phase velocity) of the various stress waves depends on the properties of the medium in which they travel; compressional wave speed is given by  $[(\lambda + 2\mu)/\rho]^{\frac{1}{2}}$ , and shear wave speed is given by  $\sqrt{\frac{\mu}{\rho}}$ , where  $\lambda$  and  $\mu$  are Lamè's constants, and  $\rho$  is the material density. In general, the wave speed (phase velocity) of Rayleigh waves is slightly less than that for shear waves in the same medium; in the particular case of a thick plate, Rayleigh wave speed is dependent on the frequency-thickness product,<sup>33</sup> a characteristic of dispersive waves. The frequency-thickness product reaches a threshold, however, beyond which the surface wave speed does not change; for steel the threshold is approximately  $1 \times 10^3$  Hz·m.

Sensors mounted on the MFTF-B superconducting magnet were excited at various distances by striking the magnet casing with a hammer;<sup>16</sup> differences of the times of arrival of the resulting stress waves were measured and an average wave speed of  $3000 \text{ m}\cdot\text{s}^{-1}$ , corresponding roughly to that of Rayleigh surface waves was reported.<sup>16</sup> One of the objectives of the GD calibration procedure was to measure accurately the speeds of stress waves propagating in the GD magnet casing.

---

<sup>32</sup>H. Kolsky, *Stress Waves in Solids*, Dover, New York (1963)

<sup>33</sup>D.C. Worlton, "Experimental confirmation of Lamb waves at megacycle frequencies," *J. Appl. Phys.* **32**, 967 (1961).

Thicknesses of various members of the GD coil casing are 85-120 mm.<sup>34</sup> As was remarked earlier, the frequencies of interest in our application are 1-50 kHz. Therefore, for the GD casing thicknesses, the Rayleigh surface wave speed for frequencies above about 10 kHz should be constant; frequencies below this threshold will have lower Rayleigh wave speeds, and therefore should not affect the determination of propagation speed. The asymptotic Rayleigh wave speed for steel is  $\approx 3100 \text{ m}\cdot\text{s}^{-1}$ .<sup>19</sup>

Wave speed in the GD coil was determined from data of the difference in arrival times for a set of two sensors plotted as a function of their separation distance. In each case, pairs of sensors were chosen so that simple determination of the distance between them could be made. Figure 15 shows the response of a sensor to calibration impacts at various distances. A small ripple can be seen to precede the Rayleigh wave arrival; the speed of this small component corresponds to a compressional wave, which is about twice the speed of the Rayleigh surface wave. The strength of the compression wave component tends to decrease in comparison with the Rayleigh wave component with increasing distance from the impact; this difference is consistent with the fact that compression waves propagate in three dimensions, while the Rayleigh waves propagate in essentially two. (The Rayleigh wave disturbance decreases exponentially with depth.<sup>32</sup>)

In generating arrival time *vs.* distance data, signals with a distinct onset of Rayleigh wave were used. Figure 16 shows that a wave speed of  $3066 \text{ m}\cdot\text{s}^{-1}$ , computed from a best-fit line (solid line) agrees well with the handbook value (dotted line).

### 3.8.3. Signal Attenuation and Broadening

As stress waves move away from their source, their intensity decreases due to spreading and dissipation. Furthermore, in a complicated structure where waves undergo many reflections, an impulsive disturbance broadens as it travels away from its source. Therefore signal attenuation and broadening may be used as additional information in locating the signal's source in the magnet.

---

<sup>34</sup>D.S. Hackley and G.S. Kruse, "General Dynamics Convair Division/Intermagnetics General Corporation design of a test coil for the Large Coil Program," *Proceedings of the 8th Symp. on Eng. Problems of Fusion Research*, IEEE Pub. No. 79CH1441-5 NPS, 1163 (1979).

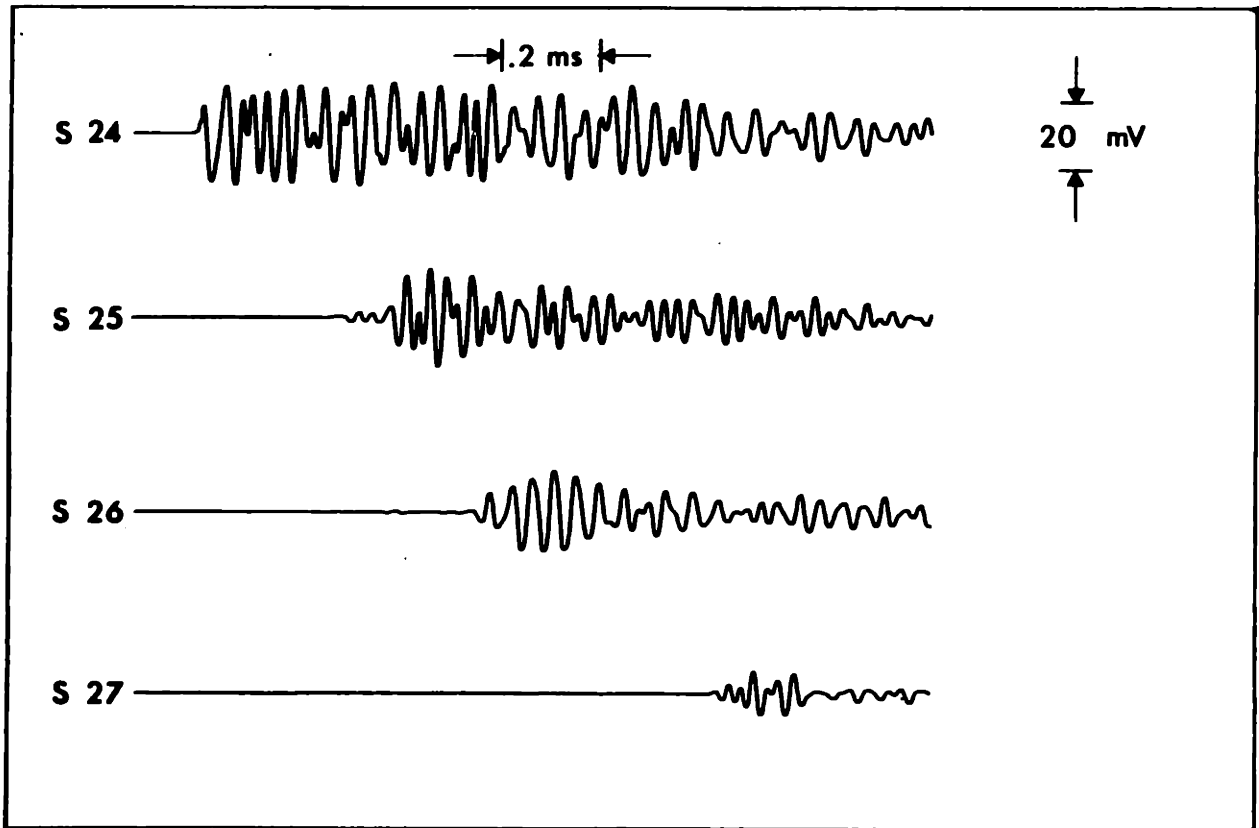


Fig. 15 Response of GD sensor 24 to calibration impact originating at locations near sensors 24, 25, 26, and 27.

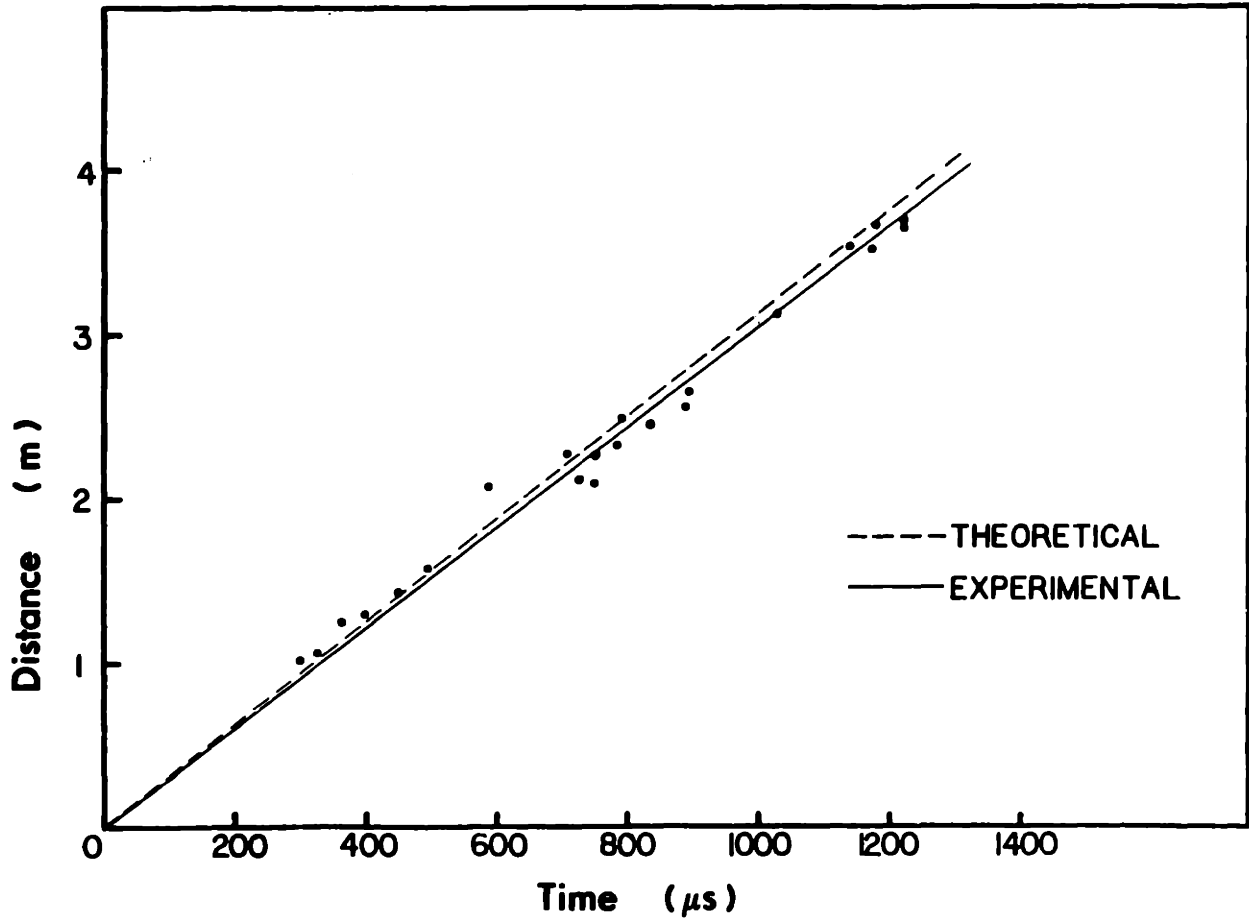


Fig. 16 Distance between calibration impact and receiving sensor vs. difference in times of arrival of calibration impact at impact location and receiver location. Slopes of lines correspond to Rayleigh wave speed.

In defining signal attenuation, the following ratio is used:

$$E/E_0 = \frac{\int_0^T V^2(t)dt}{\int_0^T V_0^2(t)dt}$$

where  $V(t)$  is the output of the sensor to a distant impact and  $V_0(t)$  is the output of the same sensor to an impact next to it;  $T$  is the duration of the signal  $V_0(t)$ . In defining signal broadening,  $T_b$  is used, the time required for the squared and integrated sensor output to reach 90 % of its final value.<sup>35</sup> The following can be concluded:

- (1) Figure 18 shows the response of sensor 24 to calibration impacts originating at locations near sensors 24, 25, 26, 27, and 5. Its response is representative of the response of any of the fifteen sensors mounted near the coil winding (sensors 15-30) in that significant signal broadening does not occur unless the signal originated near one of the peripheral sensor positions (sensors 1-10). Quantitative representations of this phenomenon are shown in Figures 18.a and 18.b , where  $T_b$  values are plotted against distance for sensors 18 and 23.
- (2) Figs. 19.a and 19.b show  $E/E_0$  vs. distance data for sensors 18 and 23.  $E/E_0$  values for impacts originating near peripheral sensors (sensors 1-10) are lower than values for impacts originating near coil winding sensors (sensors 15-30). These results are typical and it can be concluded that signal attenuation is significantly higher when the signal must travel from a peripheral location to the coil winding area than if the signal originated in the coil winding area.
- (3) Comparison of Figs. 19.a and 19.b shows  $E/E_0$  values are higher for impacts originating near sensors 23-30 and being received at sensor 23 than for those originating near sensors 15-22 and being received at sensor 18. Signals travelling along the inside face of the coil, where sensors 23-30 are mounted, are therefore attenuated less than signals travelling along the main face, where sensors 15-22 are mounted.

---

<sup>35</sup>In computing  $E_0$  and  $T_b$  values, a Nicolet digital oscilloscope was used. Signals recorded on the GD calibration tape were input to the digital scope at a sampling frequency 500 kHz. An onboard microprocessor then squared and integrated the waveform; the asymptotic value was  $E_0$ .

- (4) The signal undergoes stronger attenuation for a given distance when it must travel around a corner from one face to another, (Figs 19.a and 19.b).

#### 3.8.4. Frequency Analysis

Results of recent experiments, to be fully presented later, suggest that the coil winding in a superconducting magnet acts as a mechanical low-pass filter; thus an AE event which originates in the coil pack and propagates to the coil casing where the sensors are mounted will have lost most of the high frequency energy it originally contained. Frequency analysis, therefore, may be used to determine whether or not an event originated in the coil winding. With this in mind, the transfer function of the GD coil casing was examined. (It was hoped that there was very little high frequency attenuation so that a distinction might be made between events originating in the coil casing and the coil winding.)

FFT spectral analysis was performed on the recorded responses of various sensors to calibration impacts. The spectra can be integrated, and the frequency where 90 % of the final integrated value is reached,  $f_b$ , can be used as a measure of the distribution of frequency components.<sup>36</sup> Figure 20 shows a comparison of  $f_b$  values from the GD calibration recording and a laboratory experiment conducted on a superconducting coil winding (the full results of which are to be presented below). It can be concluded that high frequency (20-50 kHz) energy is maintained even at large distances in the GD coil casing.

---

<sup>36</sup>The Nicolet digital oscilloscope was used to compute  $f_b$  values; signals from the calibration tape were sampled at 100 kHz and transformed using the onboard FFT program. The resulting spectrum was integrated.

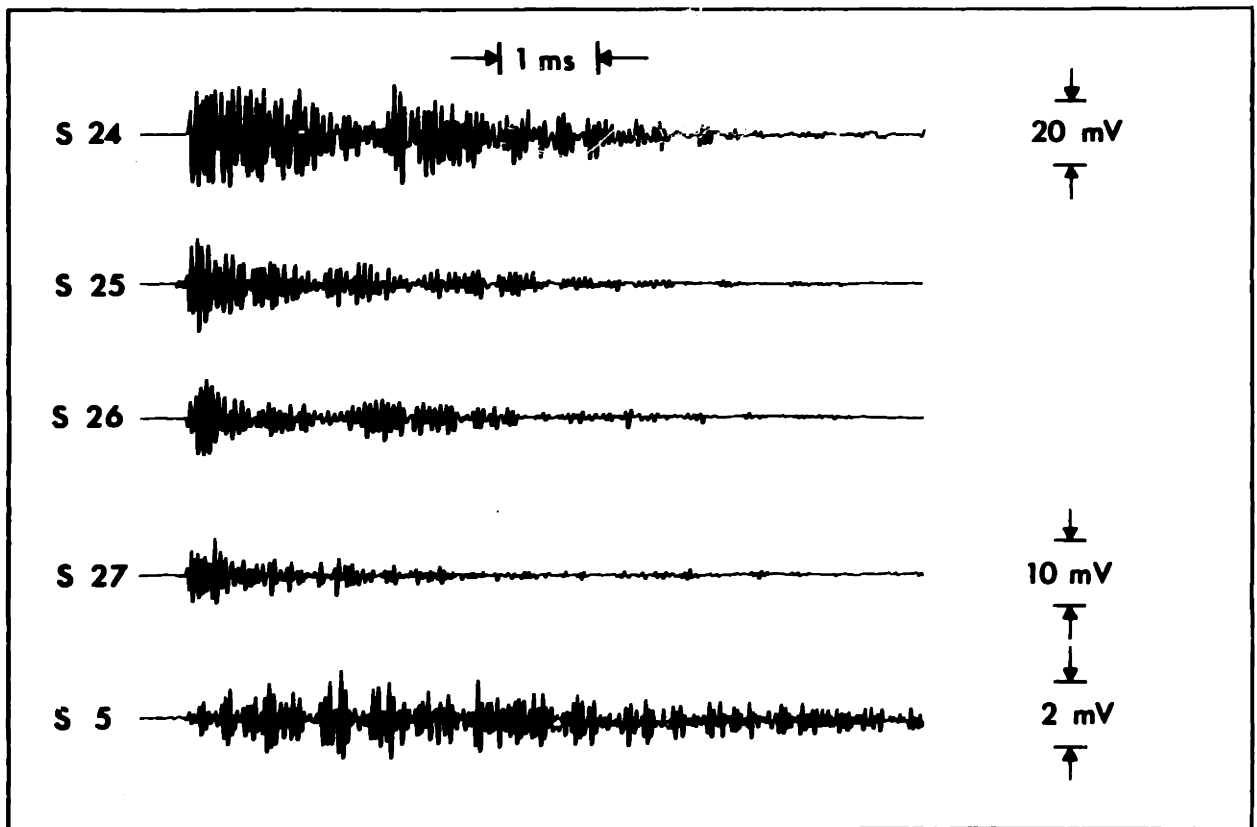


**Fig. 17** Responses of sensor 24 to calibration impact originating at locations near sensors 24, 25, 26, 27, and 5.



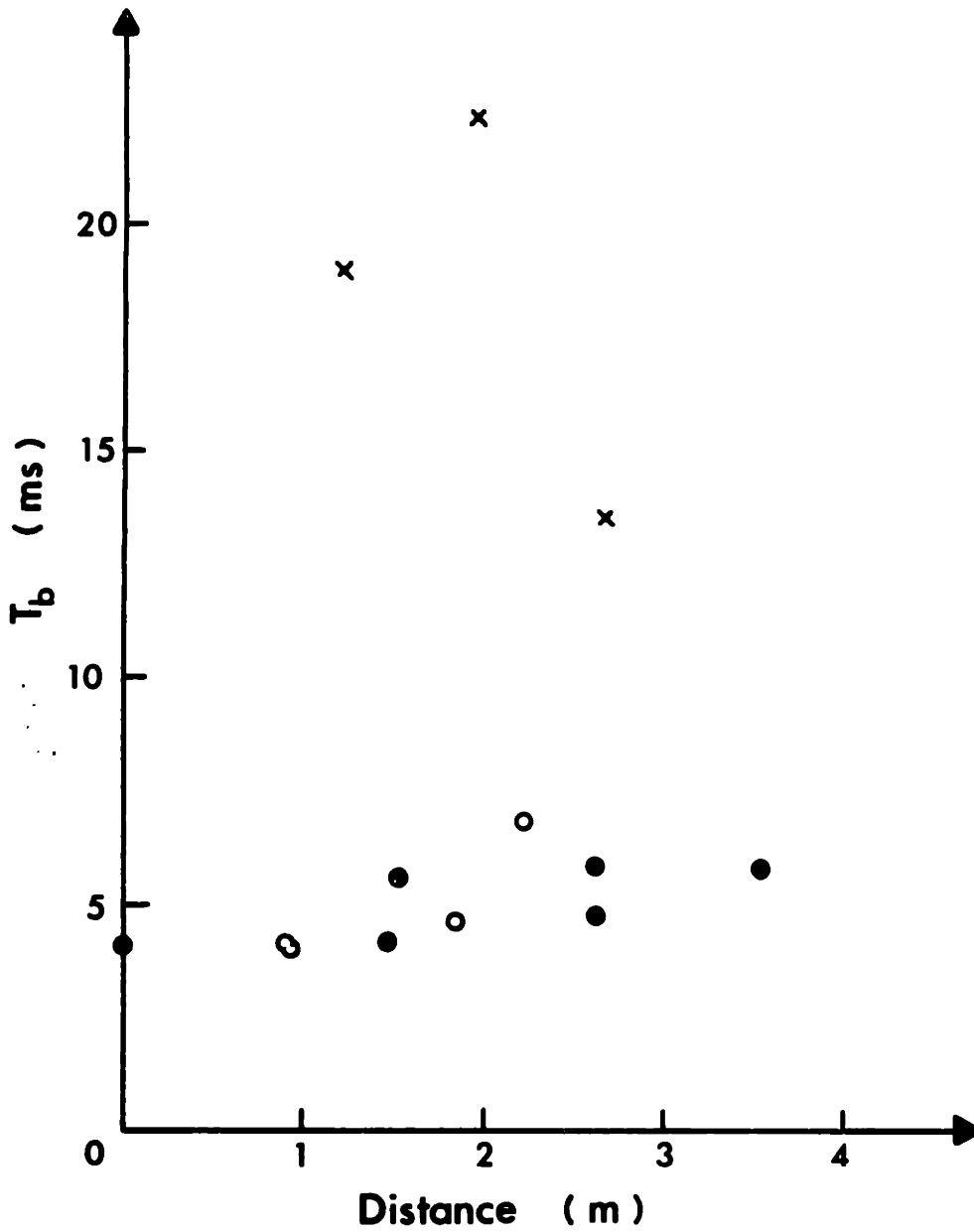


Fig. 18.a  $T_b$ , measured at sensor 18 vs. distance; origination of calibration impacts is indicated by:  $\times$  if from near sensors 1-10;  $\bullet$  if from near sensors 15-22; and  $\circ$  if from near sensors 23-30.

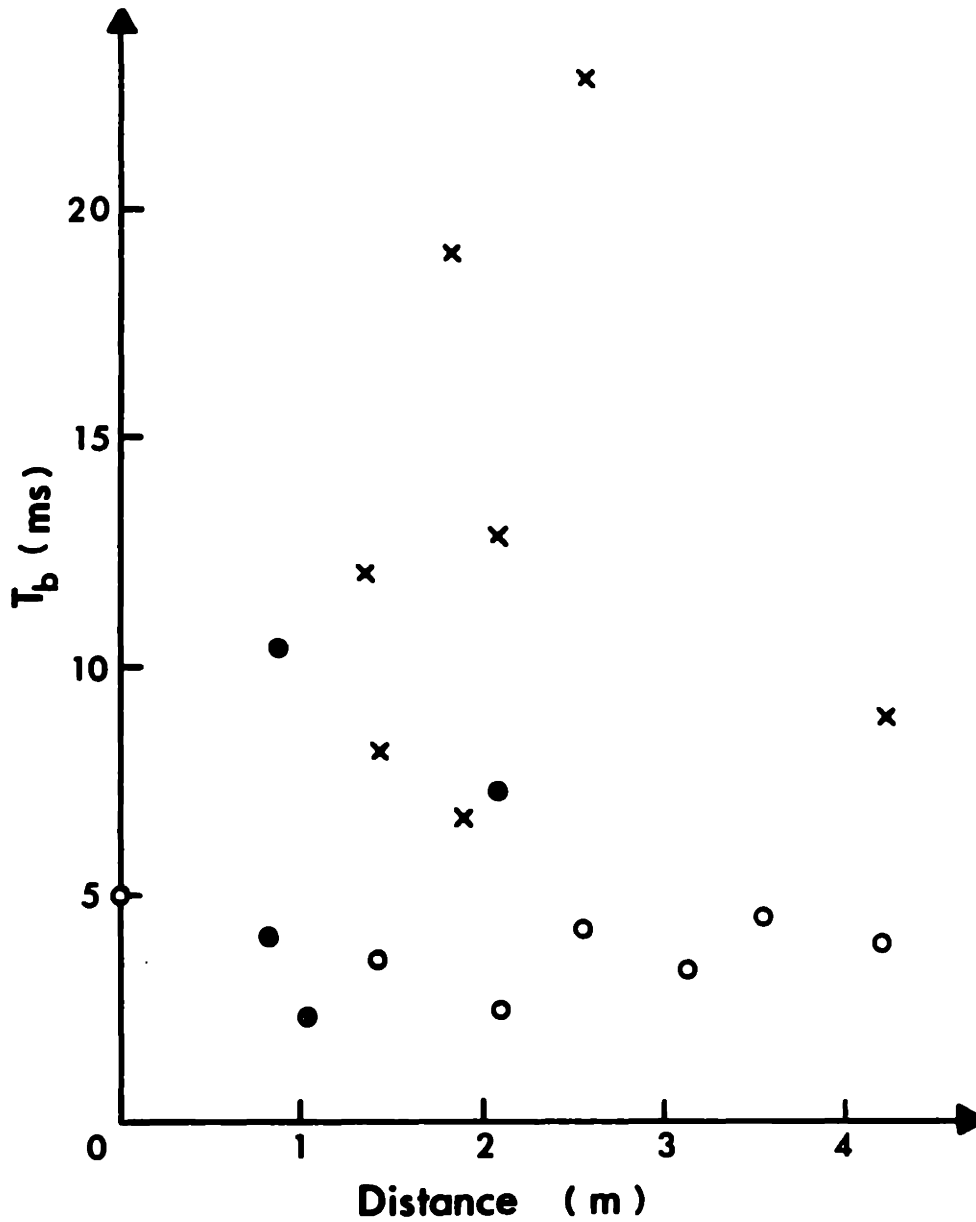


Fig. 18.b  $T_b$ , measured at sensor 23 vs. distance; origination of calibration impacts is indicated by:  $\times$  if from near sensors 1-10;  $\bullet$  if from near sensors 15-22; and  $\circ$  if from near sensors 23-30.

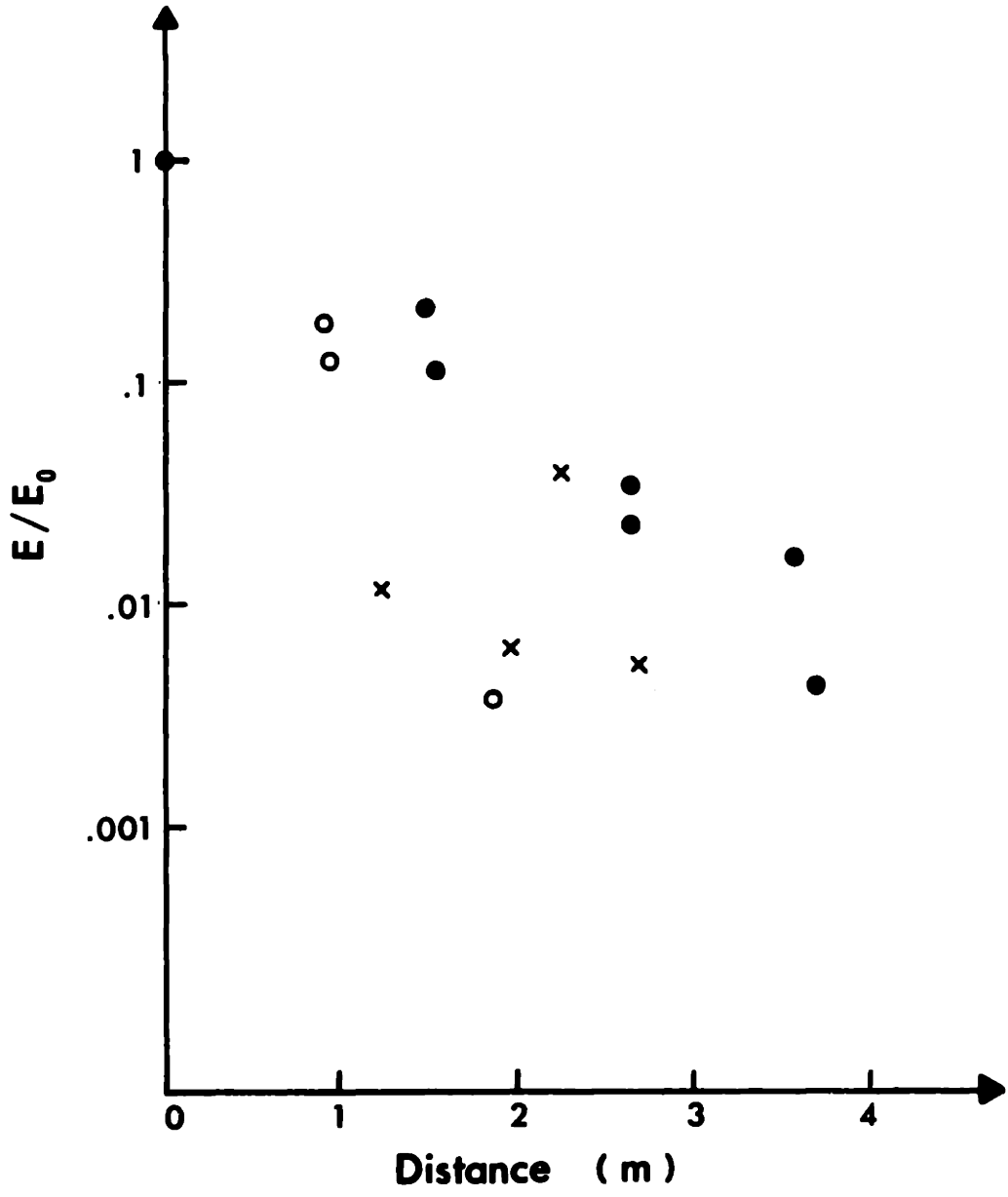


Fig. 19.a  $E/E_0$  vs. distance for sensor 18; origination of calibration impact signal is indicated by:  $\times$  if from sensors 1-10;  $\bullet$  if from near sensors 15-22;  $\circ$  if from near sensors 23-30.

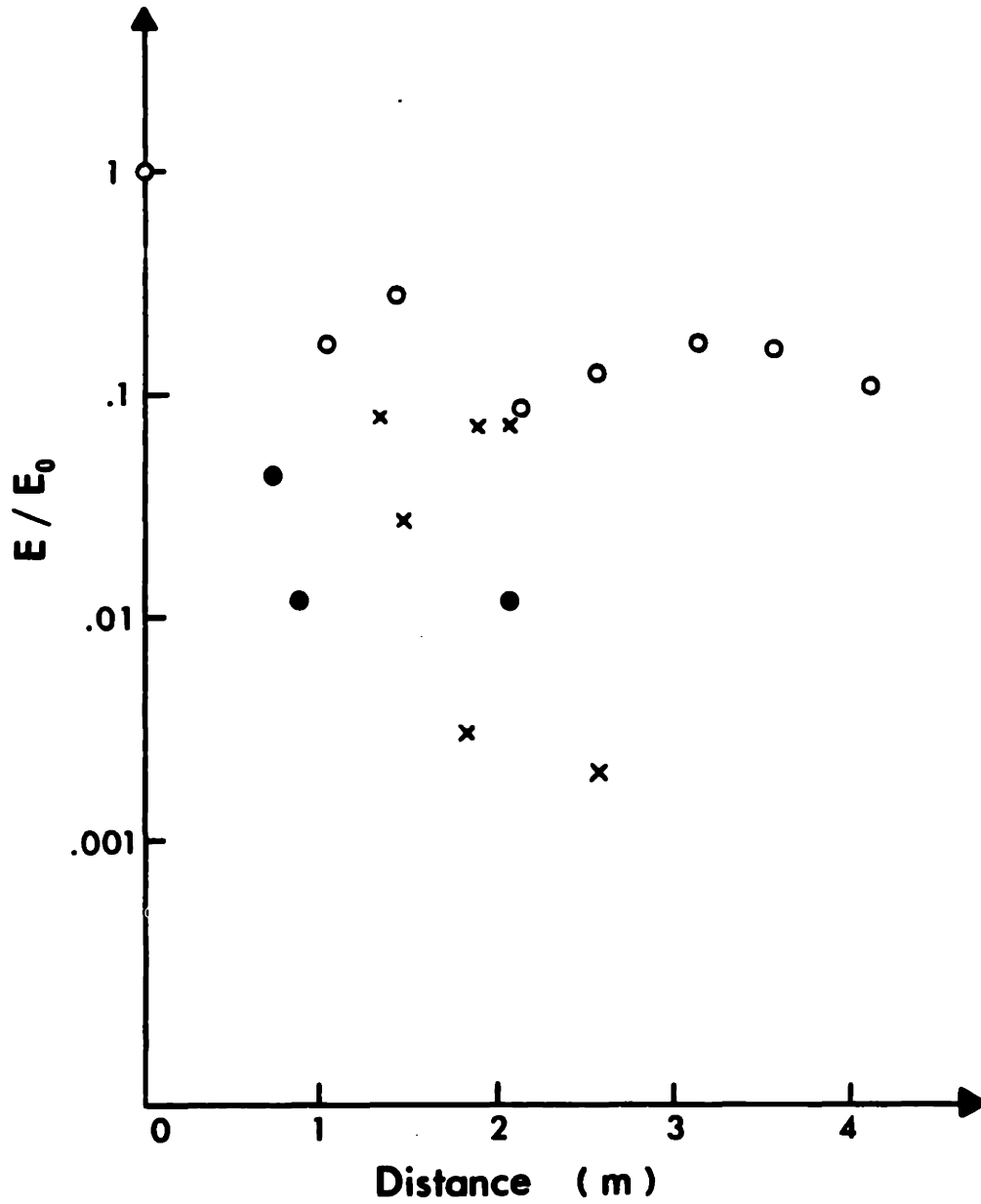


Fig. 19.b  $E/E_0$  vs. distance for sensor 23; origination of calibration impact signal is indicated by:  $\times$  if from sensors 1-10;  $\bullet$  if from near sensors 15-22;  $\circ$  if from near sensors 23-30.

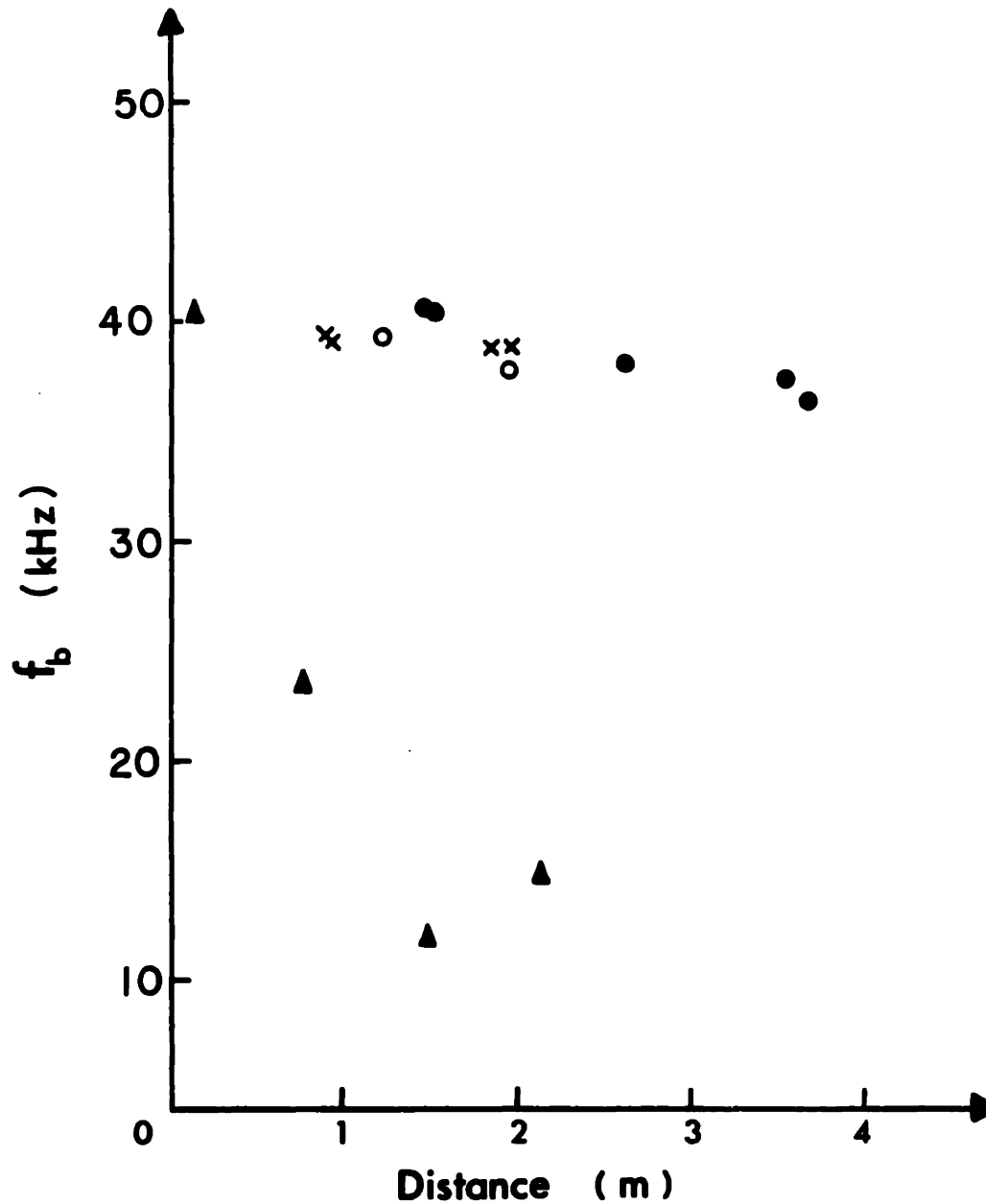


Fig. 20  $f_b$  vs. distance for sensor 18; origination of calibration impact signal is indicated by: × if from sensors 1-10; ● if from near sensors 15-22; ○ if from near sensors 23-30. Note: the data from the laboratory coil winding have been extapolated to compare with the GD data; in other words, distance was scaled, based on the number of winding turns per unit distance for the experimental winding and the GD coil.

## 4. DATA PROCESSING AND ANALYSIS

### 4.1. Wave Propagation Research

Fundamental to the interpretation of acoustic emission data is an understanding of wave propagation. Until recently, AE data from large superconducting magnets have been used principally to identify and locate conductor-motion events. Triangulating the source of AE events hasn't been attempted partly because little is known about wave propagation in the magnet winding and structure. Experiments described below present data useful in understanding this subject.

#### 4.1.1. Wavefront Propagation in a "Pancake" Winding

Figure 21 shows the coil winding used in the following experiments. The winding is a single layer, or "pancake," of a multilayer superconducting magnet.<sup>37</sup> Thin fiberglass spacers separate the turns of the winding. Appendix E contains some important dimensions of the coil which are pertinent to these experiments.

One experiment generated contours of the wavefront initiated by an impulse applied at the innermost turn of the winding. A sensor was mounted next to the impact point to mark the impact instant and a second sensor, movable to any point on the magnet surface, sensed the propagating wave front. The sensors outputs were recorded by a waveform digitizer, from which time delay between the impact instant and the arrival of the wavefront could be determined. By probing with the movable sensor for positions of equal delay, contours of the spreading wavefront could be generated. Data clearly show that the wave front speed in the radial direction is very much slower than the speed along the conductor (the cylindrical direction).<sup>38</sup> A simple model based on the two orthogonal wave velocities can be used to produce theoretical wave front contours in two dimensions. Figure 22 shows experimental and theoretical contours at one instant: agreement between data and theory is good.

---

<sup>37</sup>M.J. Leopold, T. Weggel, and Y. Iwasa, "Design and operation of 25.4 and 30.1 tesla hybrid magnet systems," Proc. Sixth Int'l Conf. on Magnet Technology (MT-6), (Alfa Press, Bratislava) 401 (1978).

<sup>38</sup>Wave speed in the radial direction is about  $1000 \text{ m}\cdot\text{s}^{-1}$  and about  $5000 \text{ m}\cdot\text{s}^{-1}$  in the cylindrical direction.

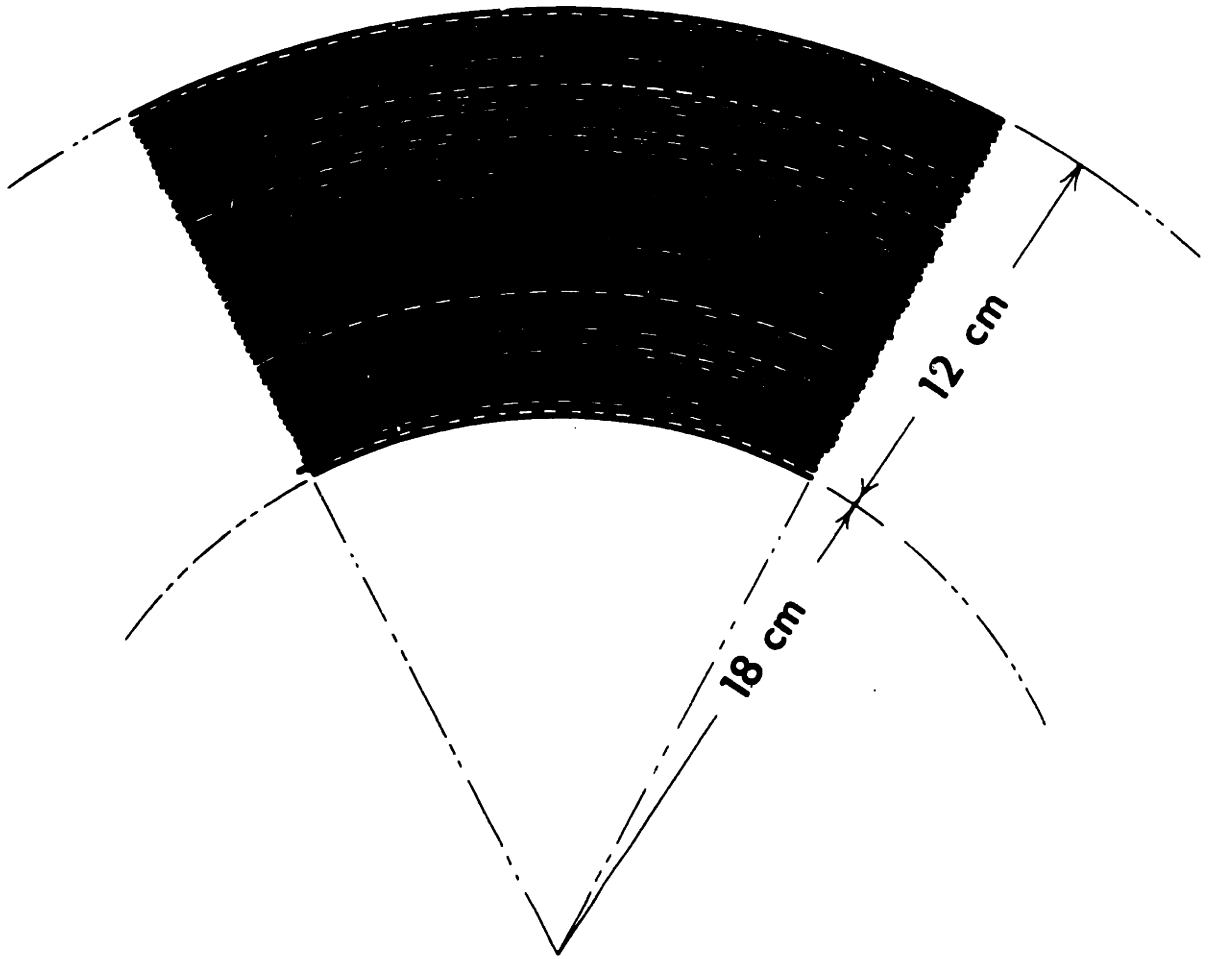


**Fig. 21** Schematic of pancake coil winding used in wave propagation experiments.

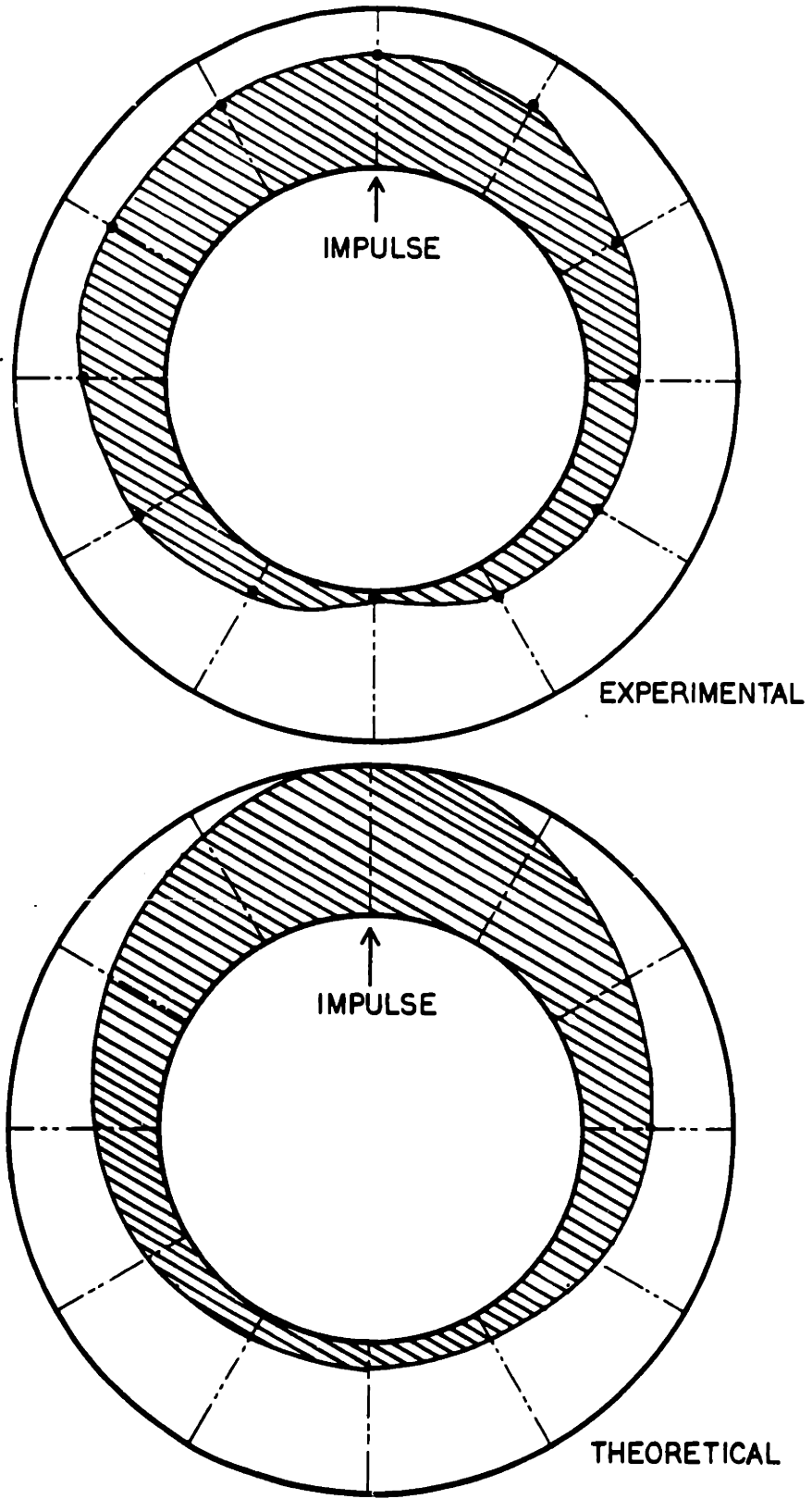


**Fig. 22** Experimental and theoretical contours showing location of stress wavefront resulting from an impact to an experimental coil winding.



Propagation speed along a third direction, mutually orthogonal with the first two, was determined by using the whole coil, made up of 38 pancakes identical to the one used above and separated by 2-mm thick fiberglass spacers. Data can be fitted well with the above model by adding the third component of velocity.

#### **4.1.2. High-Frequency Attenuation in a Magnet Winding**

Another experiment determined the frequency-dependent attenuation of stress waves propagating through a single pancake of the coil used above. The coil was excited by driving an AE sensor mounted on the innermost turn of the coil with a continuously-variable sinusoidal signal. A pickup sensor was mounted to a thin metal plate (7 cm x 3 cm x 15 mil) which could be tapped down between any two turns of the winding, thereby facilitating the transmission of mechanical vibrations induced in the coil to the pickup sensor. The experiment was conducted at both room temperature and 77 K.

The results, presented in Fig. 23, show strong attenuation for frequencies above 20 kHz, but little or no attenuation below this frequency. In addition, it can be seen that most of the attenuation takes place within a short distance of the driving sensor. The experiment was repeated for a transient excitation. FFT spectra from the pickup sensor were generated, and again, frequencies above 20 kHz were strongly attenuated.

#### **4.1.3. Discussion of Results**

If the result that high frequencies are attenuated in the coil winding used can be generalized to most magnets, it will mean that AE events coming from within the coil winding may be identified by their distinct lack of high frequency components. Ideally, the degree of high frequency attenuation may be used as a measure of the depth of the initial disturbance in the winding.

Furthermore, if triangulation techniques for localizing acoustic emission events are to be developed for complicated superconducting magnet systems, a knowledge of propagation paths and speeds is essential. The fact that stress waves travel much more slowly in the radial and vertical (through the stack) directions for the winding used may be generalized to most other magnets.

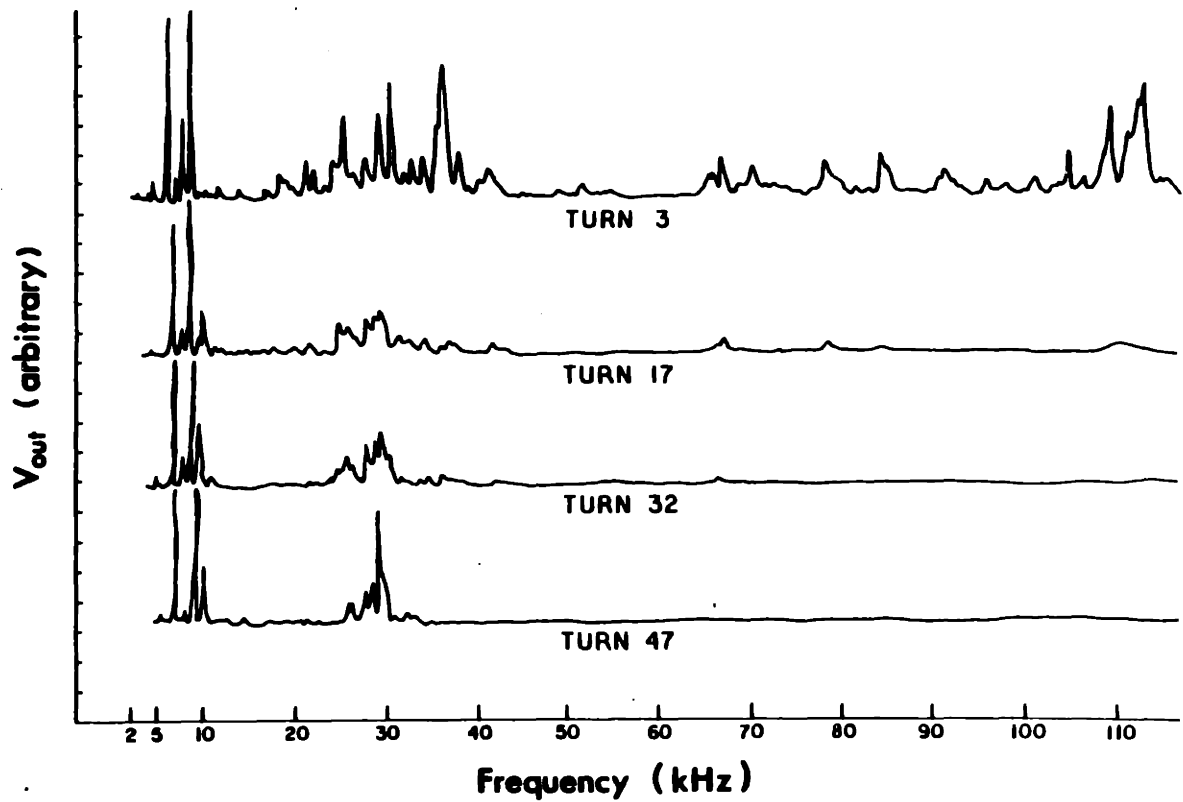


Fig. 23 Frequency response across 3, 17, 32, and 47 turns of pancake coil.

## **4.2. LCP Data Analysis Recommendations**

Whereas in the past acoustic emission monitoring of superconducting magnets has been possible only for isolated magnet testing sequences, the LCP offers the first opportunity to use AE monitoring techniques over an extended magnet testing period. A data base for the recognition of long-term trends therefore may be possible; data from the GD and other LCP coils should be processed and analyzed with this in mind. More specifically, plots should be generated showing the distribution and energy density of both conductor-motion and structural-motion-induced AE events. In addition, the results of other diagnostic techniques should always be incorporated to complement and corroborate AE diagnostic results.

Although the verification of the long-term structural integrity of magnets from AE data is one of our primary objectives, short-term diagnostic techniques should also be developed. As was remarked earlier, the LCP magnets are designed to be stable; however, in an experimental program of this scale, and with the number of different and sometimes novel magnet designs,<sup>29</sup> there is some possibility of magnet failure or at least of unforeseen problems which cause interruption of magnet operation. It would be very useful if acoustic emission techniques could ultimately identify and in some cases forewarn these interruptions. Therefore, LCP data should be correlated with data from other magnet monitoring techniques in order to establish its usefulness.

The LCP also presents the opportunity to develop new data analysis techniques based on laboratory experiments. Because the LCP schedules did not permit the acquisition or analysis of data from the GD coil for this thesis work, recommendations for data analysis based on work presented here follow.

The number and configuration of sensors on the GD coil should make it possible to improve the accuracy in determining the location of AE events. In particular, structural events should be recognized by their first arrival at peripheral sensor positions (1-10). Determination of the origin of other structural events, namely those originating in the coil casing, the immediate coil structure, or the coil pack may be accomplished by frequency analysis; if the spectra consist mostly of low-frequency components, experiments presented above suggest that they have travelled through the coil winding and have thus originated there. In addition, a structural event originating within the

coil pack should take much longer to arrive at the nearest sensor than those originating outside the coil pack and travelling along the coil casing. The increased time delay and the absence of high frequency components should be sufficient to classify these events as coming from the coil pack and not the coil casing.

Conductor-motion-induced AE events can be recognized by the simultaneous presence of a voltage pulse, but other techniques should be incorporated to improve the determination of their origin. Possible techniques include: (1) frequency analysis (FFT) to determine whether their spectra are indicative of their depth in the coil winding, and (2) arrival time differences should be analyzed for evidence of elongation due to the disturbance having to travel across conductor turns.

As was remarked earlier, if we are to interpret AE signals more quantitatively, a measure of their energy content should be developed. It has been shown that sensors mounted on different parts of the magnet receive significantly different amounts of energy from the same calibration impact. Therefore, a sensor's response to an AE event should be normalized against its calibration response.

Finally, when AE data are processed according to sensor channel number, time of occurrence, energy content, duration ( $T_b$ ), and frequency composition ( $f_b$ ), data may be presented in a variety of ways. These include: (1) AE event counts versus magnet current, (2) AE activity as a function of event location, and (3) plots correlating AE event energy with magnet current, charging sequence, and location.

### **4.3. Signal Processing Recommendations**

Distinct AE events recorded during a charging sequence typically number in the thousands.<sup>12</sup> Manual signal processing is an impractical solution to signal processing needs since even the most basic signal processing techniques, such as event counting, would be cumbersome. Clearly, with the number of events typical in this application, some sort of automatic signal processing system is necessary.

#### **4.3.1. Analog Signal Processing**

Our first efforts to process multiple-event AE data used an analog signal processor, a device capable only of counting AE events. To be counted as an event, the signal had to

exceed a threshold; when this occurred, a counter incremented, and a "window" of time opened during which the device would not respond to other signals so that the initial AE event could decay below the threshold. Numerical data from the counters were then copied by hand. The device worked adequately in cases where AE event counts were considered the only significant parameter, but the device had obvious limitations: (1) most importantly, the processor was limited to counting AE events; subsequent research has centered on the classification of AE signals by signal analysis techniques, requiring more sophisticated signal processing, (2) bulk and expense prevented the use of more than two channels simultaneously, making multichannel signal processing impractical, and (3) noise affecting the sensor signals could be mistaken by the processor as an AE event; (for example, the analog processor would have been useless on MFTF-B data, where periodic noise spikes were of the same order of magnitude as the AE signals.)

#### **4.3.2. Analog/Digital Signal Processing**

It is possible to design and build more sophisticated analog circuitry to overcome some of these problems, but it has become clear that a combined analog/digital signal processor capable of advanced signal processing and compatible with a modern computer ultimately would be the most practical and flexible type of AE signal processor. Jozef Lore<sup>16</sup> demonstrated the feasibility of such an advanced analog/digital signal processor for use on the particularly troublesome AE data from the MFTF-B magnet. Although some of the circuitry was designed specifically to recognize and discard the periodic noise spikes superimposed on the MFTF-B sensor signals, some features of the circuit can be applied to future systems where more general data processing capabilities will be necessary. These features include: (1) expandability to multiple channels, (2) interface to the DEC PDP 11/23 minicomputer, (3) noise filtering capability, (3) automatic correlation of AE events with magnet voltage transients, thus allowing the recognition of conductor motion events, and (4) variable threshold settings on each channel.

With this preliminary experience in mind, and with recent developments in the understanding of acoustic emission mechanisms, we have undertaken the task of developing a new analog/digital signal processing system capable of handling a variety of data from different magnet systems.

#### 4.4. Development of Analog/Digital Signal Processor

Although it is unlikely that analog AE recordings will ever become totally obsolete — they will always be useful for visual representation of AE signals and as backups to digital recordings — it is our belief that the advantages of digital signal processing and analysis are particularly well suited for both long and short-term acoustic emission monitoring of superconducting magnets. Work has begun towards developing such a system and the following objectives have been defined:

- (1) *AE event parameterization.* The amount of computer memory necessary to completely store an AE event is prohibitive. For example, a signal which has useful information contained in a frequency band whose upper limit is 100 kHz would require a sampling frequency of no less than 200 kHz; a typical AE event lasting 20 ms would therefore require at least 4000 memory locations. In any case, the continued use of analog recordings will preserve the time history of the AE events within the limits of the recorder's frequency response. Much better suited to digital storage is the parameterization of AE events — that is, performing initial signal analysis in order to distill its important parameters, then storing the numbers which represent these parameters. Some obvious examples of these parameters would be the event's sensor channel number, peak amplitude, rise time, duration, fundamental frequency, and time of occurrence. Other less obvious examples might be parameters based directly on the results of recent experiments on wave propagation in superconducting magnets. For example, a parameter might represent the degree to which the high frequency components of an AE event have been attenuated (see section 4.1.).
- (2) *Flexibility.* The system should not be developed for a particular magnet system, but should be adaptable to any large magnet system.
- (3) *Portability.* The system should not rely on either equipment which is too difficult to transport or software which is incompatible with computer systems common to most large superconducting magnet facilities. In other

words, the data acquisition portion of the system should be self-contained and portable.

- (4) *Noise Filtering.* Because each superconducting magnet system has associated with it its own type of noises, and because some of these noises can be particularly troublesome in regard to signal processing, the digital signal processor must have sophisticated and flexible noise filtering capabilities. They should include the ability to filter noise of the type affecting MFTF-B data recordings (periodic spikes) and continuous background noise, either electrical or acoustic.
- (5) *Real time display.* In many cases, the ability to display (in real time) analyzed or partially analyzed AE data is important. For example, superconducting dipole magnets for high energy physics applications will emit, when energized, acoustic signals proportional to the degree of symmetry in their winding; because this symmetry is extremely important to the performance of the magnet, a real time diagnostic technique capable of displaying this asymmetry is particularly useful.
- (6) *Storage capacity.* Whatever method of storing digitized parameters of AE events is used, its capacity should be large enough that storage memory does not have to be replenished often during a magnet charging sequence. (Either a hard or floppy disc storage system usually fulfills this requirement easily.)
- (7) *Expandability.* Because different magnet systems and different experimental objectives require different numbers of AE sensors, the system should be capable of accompanying varying numbers of sensors. (The largest number of sensors used on a magnet to date is the thirty currently mounted on the GD-LCP coil.)

#### **4.5. Software-based Data Analysis**

The integration of AE signal processing hardware with a modern computer allows the use of software programs to analyze AE data. While it has been possible for some time to enter data by hand into a computer's memory and then instruct the

computer to perform operations on that data, it is more practical to enter the output of signal processing hardware *directly* into the computer's memory, thus saving a time-consuming step. The number of parameters necessary to describe an AE signal accurately is relatively small, and thus common minicomputer storage systems can easily hold large amounts of processed AE data. Once stored, computer programs ranging from the most elementary (event counting) to the most sophisticated (graphics routines) are possible. Furthermore, both long and short term trends can be recognized quickly by the proper programs: it will be possible, for example, to process huge amounts of data — possibly accumulated over years of magnet testing — in order to identify long term trends that would have represented intractable amounts of manual work in the past; similarly, "fast" programs can be used in order to identify potentially hazardous short-term magnet behavior.



## 5. SUMMARY AND CONCLUSIONS

Key achievements of the work presented here may be summarized as follows:

- (1) Thirty AE sensors were placed strategically on the General Dynamics LCP coil. With this configuration, we expect to distinguish the source and location of disturbances generating AE signals.
- (2) A room-temperature calibration procedure was conducted on the thirty differential AE sensors mounted on the GD coil. A repeatable impact was delivered to various locations on the coil casing and the sensor responses were recorded on the multichannel tape machine. The results of the calibration will allow more accurate interpretation of LCP AE data in addition to having helped establish several new methods of AE signal analysis.
- (3) Results of wave propagation experiments conducted on a two and three-dimensional coil winding are : 1) Contours of wave fronts can be generated and show that the waves propagate in three orthogonal directions, each with a distinct velocity which depends on the average properties of the materials the waves must pass through in the three directions, and 2) high frequency components are severely attenuated as the disturbance travels in the radial or vertical directions.
- (4) A differential sensor with an improved signal-to-noise ratio has been developed. The expected improvement in the sensor's performance should permit the use of more sophisticated signal processing and data analysis techniques.

## 6. APPENDICES

### 6.1. Appendix A: Differential Sensor Construction

(Refer to Figure 5)

Channel Industries grows 2-mm thick by 10-mm diameter piezoelectric crystal discs which it then cuts into two half-moon pieces. The crystal is made of lead titanate zirconate type PZT 5A.

The copper tubing is placed through the hole in the pipe cap and the two are then silver soldered together. The copper foil disc and the brass shoe disc are cut from stock. The copper foil disc is coated with flux and tinned on one face. (SN-62 low temperature solder should be used throughout the sensor's construction.) The brass shoe disc is tinned on a 3-mm band on the outside of one face.

The two crystals, one with its positive side facing up and the other with its negative side facing up, are placed in a plastic jig which holds them firmly in the configuration in which they will be soldered to the foil disk. The two crystal faces showing are coated with flux and tinned. The foil disk, tinned side down, is then centered on the two crystals, and the soldering iron is gently swept across the untinned side of the foil disk for approximately one minute. The assembly of the two crystals soldered to the foil disk is then removed from the jig and inspected. There should be no visible gaps between the crystals and the foil; debonding of the crystal from the foil is the most common cause of sensor failure, thus making this a crucial step.

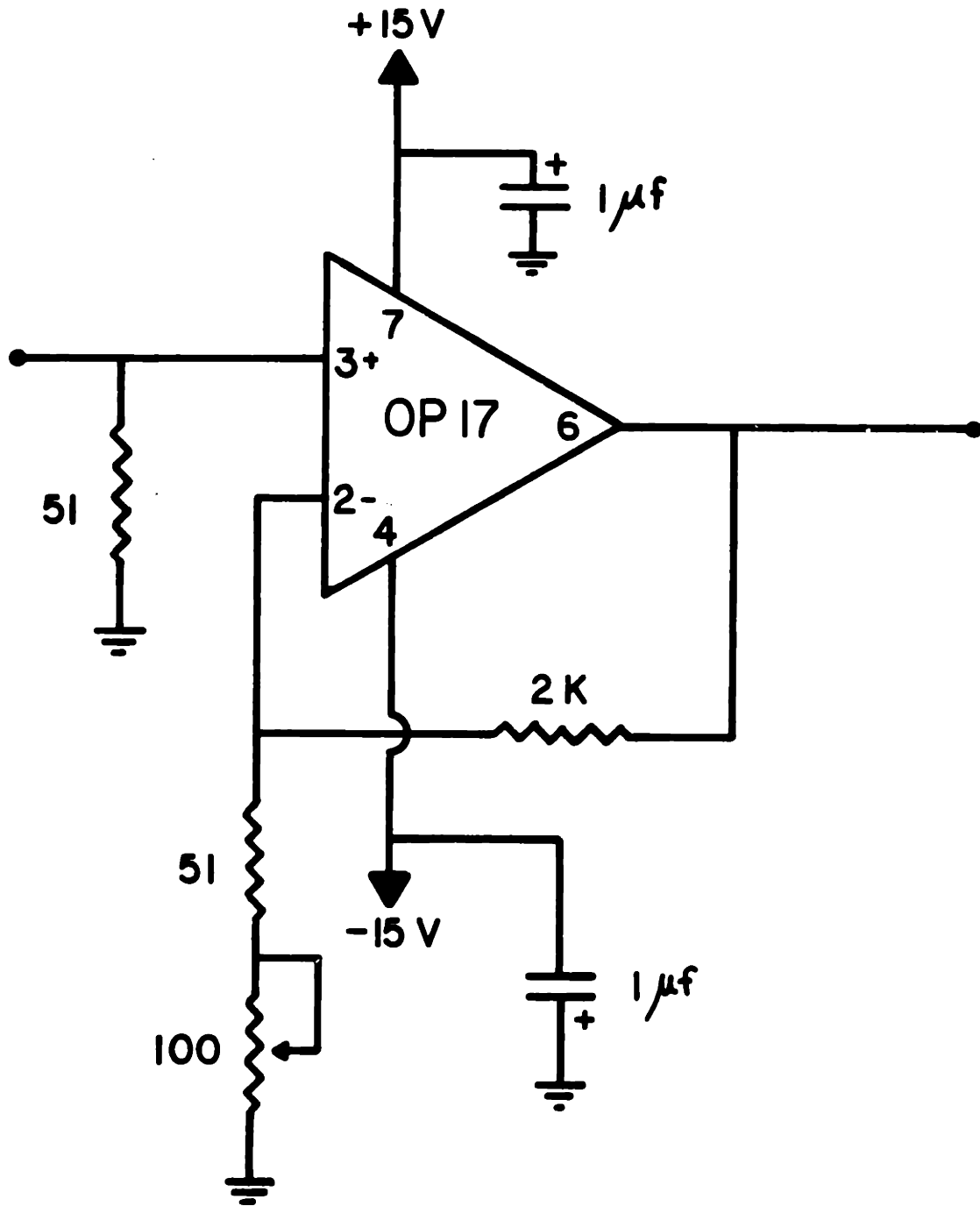
On each of the untinned faces of the two crystals, a dab of flux and then a bead of solder is applied. A teflon jacketed twin-axial cable (Belden 83315 or equivalent) is then stripped back and the two lead wires fed through the copper casing assembly, and the leads soldered to the two solder beads on the crystals.

The resulting assembly — the crystal-foil assembly now soldered to the twin-axial copper casing assembly — is then sandwiched with the brass shoe in a clamping jig. At this point the two signal cables and the ground shield are

checked for shorts. When there are none, a soldering iron should be applied to the area where the brass shoe and copper foil meet the copper casing, and a solder bead laid down around the circumference of this final assembly. As the assembly becomes hot, the bead will begin to flow, and the iron should be used to smooth and even it. It is very important that the whole assembly be allowed to cool before it is moved, because it is possible for the lead wires to be loosened from their connection to the crystals. When the assembly has cooled sufficiently, the ground shield is trimmed and tucked into the space left in the tubing opening, and the shield soldered in place. Once again, the sensor should be allowed to cool and then checked for shorts, although if one exists, the entire sensor will have to be scrapped and only the crystals salvaged.

The basic AE sensor is now complete, and its termination to a convenient connector is all that remains.

## 6.2. Appendix B: Secondary Amplifier Circuit Diagram



### 6.3. Appendix C: General Dynamics LCP Magnet<sup>34</sup>

- (1) *Magnet structure.* An exploded view of the coil structure is shown in Figure 24. It is made entirely of 304L stainless steel, a decision based on the material's mechanical and physical properties, principal among which are weldability, ruggedness at cryogenic temperatures, and low cost. The magnet structure is somewhat unique in that it is all-welded.
- (2) *Conductor.* Figure 24 also shows a perspective of the conductor; a deep channel is cut into an I-shaped copper piece in which copper-stabilized NbTi superconductor is run. The sides of the I-shaped conductor are finned to allow high heat transfer from the conductor to the liquid helium. The conductor has a current-carrying capacity of at least 13,000 A at 8 T, which is 30 % above the conductor's critical current at this field.
- (3) *Winding technique.* The coil is wound in layers, from the inside out. The conductor is strained the "hard-way," or "edge-wise" — in other words, the long axis of the "I" lies in the radial direction. Each turn and each layer of the winding is separated by fiberglass spacers which electrically insulate the conductor and at the same time allow the passage of liquid helium. Crossover points from one conductor layer to the next are located in the lowest stress regions (the high radius curves on the outside-top and bottom of the coil).
- (4) *Helium cooling system.* The magnet is pool-cooled; in other words, the conductor winding sits in a quasistatic bath of liquid helium.

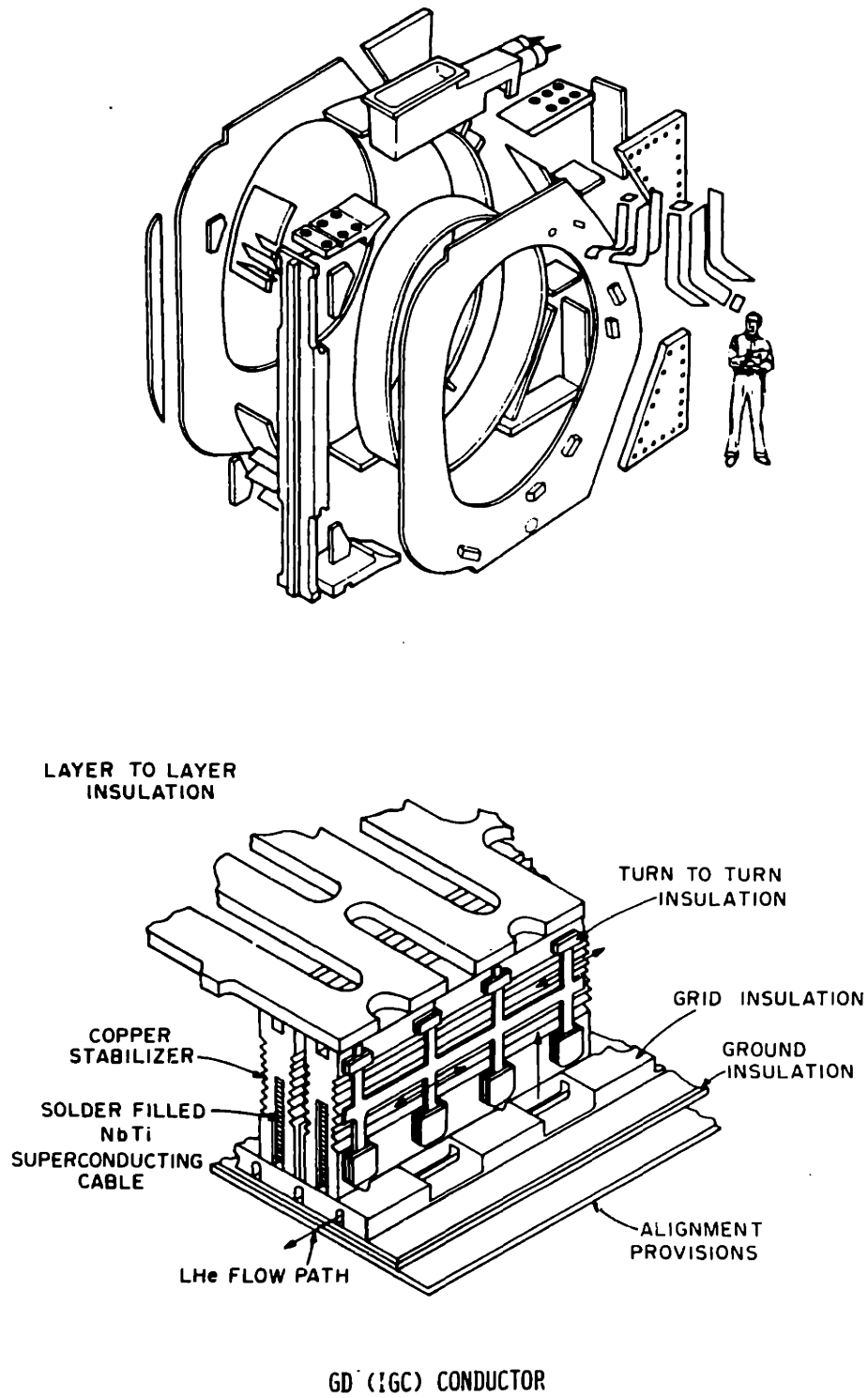


**Fig. 24** Exploded view of GD coil structure (top) and perspective view of GD conductor and winding insulation (bottom).

#### 6.4. Appendix D: GD Sensor Coordinates

Refer to Fig. 25 for the origin of the coordinate system and a schematic of the sensor locations.

| <u>Sensor</u> | <u>X (m)</u> | <u>Y (m)</u> | <u>Z (m)</u> |
|---------------|--------------|--------------|--------------|
| 1†            | 3.20         | 1.00         | -.50         |
| 2†            | 3.20         | 1.00         | .50          |
| 3†            | 3.20         | -1.00        | -.50         |
| 4†            | 3.20         | -1.00        | .50          |
| 5             | .15          | -1.98        | -.22         |
| 6             | .15          | -2.00        | .22          |
| 7             | .15          | 2.03         | -.22         |
| 8             | .152         | .04          | .22          |
| 9             | 2.31         | 2.76         | -.36‡        |
| 10            | 2.26         | 2.73         | .36‡         |
| 11†           | .15          | -2.05        | -.50         |
| 12†           | .15          | -2.05        | .50          |
| 13†           | .15          | 2.05         | -.50         |
| 14†           | .15          | 2.05         | .50          |
| 15            | 2.22         | 1.78         | .37          |
| 16            | 3.21         | .74          | .37          |
| 17            | 3.25         | -.53         | .37          |
| 18            | 2.32         | -1.68        | .37          |
| 19            | .81          | -1.64        | .37          |
| 20            | .34          | -.49         | .37          |
| 21            | .33          | .54          | .37          |
| 22            | .85          | 1.73         | .37          |
| 23            | 1.49         | 1.71         | -.06         |
| 24            | 2.68         | 1.06         | .09          |
| 25            | 3.04         | .06          | .19          |
| 26            | 2.76         | -.95         | .09          |
| 27            | 1.44         | -1.65        | .13          |
| 28            | .76          | -.99         | .07          |
| 29            | .71          | .03          | .25          |
| 30            | .76          | 1.05         | .07          |

---

† Sensor was not mounted at time of calibration. These values are within 20 %.

‡ These coordinates were difficult to measure and are within 10 % .

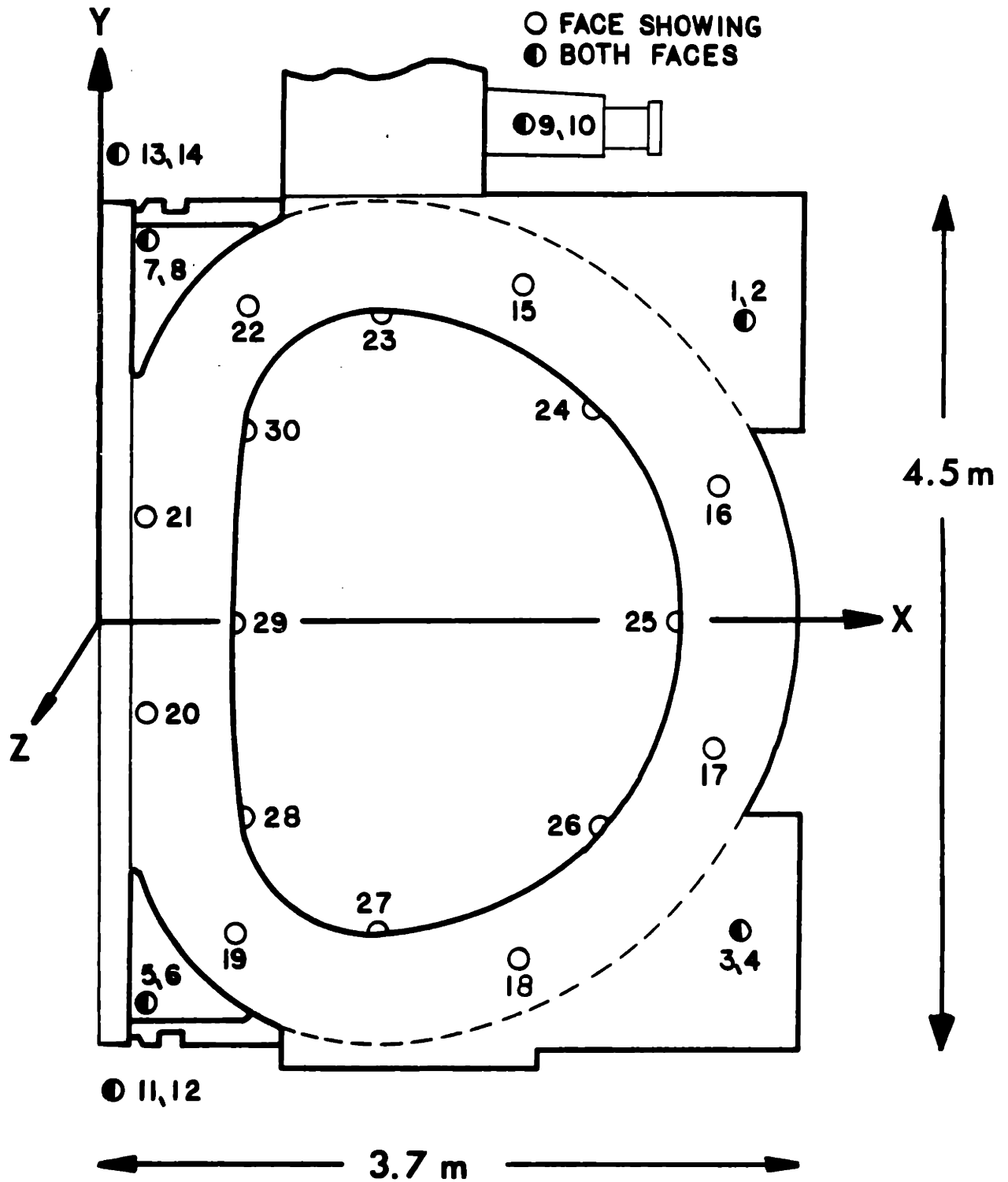


Fig. 25 Origin of coordinate system for sensor locations on GD coil. Origin of Z-axis is at midplane of coil.



## 6.5. Appendix E: Pancake Coil Parameters

Refer to Figure 21.

|                    |       |
|--------------------|-------|
| Inside diameter:   | 360 m |
| Outside diameter:  | 300 m |
| Pancake thickness: | 10 mm |
| Total turns:       | 52    |
| Spacer thickness:  | .4 mm |
| Spacer height:     | 10 mm |
| Spacer width:      | 3 mm  |

## 6.6. Appendix F: LCTF Feedthrough Plug Pin Assignment

### PLUG I

| <u>Pin</u> | <u>Sensor</u>                | <u>Wire Color</u>  |
|------------|------------------------------|--------------------|
| A          | Ground                       | —                  |
| B          | Ground                       | —                  |
| C          | —                            | —                  |
| D          | 15 <sub>2</sub> <sup>†</sup> | black <sup>‡</sup> |
| E          | 15 <sub>1</sub>              | green              |
| F          | 14 <sub>2</sub>              | black              |
| G          | 14 <sub>1</sub>              | red                |
| H          | 13 <sub>2</sub>              | green              |
| J          | 13 <sub>1</sub>              | red                |
| K          | 12 <sub>2</sub>              | green              |
| L          | 12 <sub>1</sub>              | white              |
| M          | 11 <sub>2</sub>              | blue               |
| N          | 11 <sub>1</sub>              | red                |
| P          | —                            | —                  |
| R          | 10 <sub>2</sub>              | red                |
| S          | 10 <sub>1</sub>              | yellow             |
| T          | 9 <sub>2</sub>               | brown              |
| U          | 9 <sub>1</sub>               | red                |
| V          | 8 <sub>2</sub>               | red                |
| W          | 8 <sub>1</sub>               | orange             |
| X          | 7 <sub>2</sub>               | black              |
| Y          | 7 <sub>1</sub>               | white              |
| Z          | 6 <sub>2</sub>               | brown              |
| a          | 6 <sub>1</sub>               | green              |
| b          | 5 <sub>2</sub>               | black              |
| c          | 5 <sub>1</sub>               | brown              |
| d          | 4 <sub>2</sub>               | green              |
| e          | 4 <sub>1</sub>               | blue               |
| f          | 3 <sub>2</sub>               | red                |
| g          | 3 <sub>1</sub>               | blue               |
| h          | 2 <sub>2</sub>               | green              |
| j          | 1 <sub>2</sub>               | black              |
| k          | 2 <sub>1</sub>               | yellow             |
| l          | 1 <sub>1</sub>               | orange             |
| m          | Ground                       | —                  |

<sup>†</sup> The 2 subscript refers to the black lead from the sensor, the 1 to the white lead.

<sup>‡</sup> The wire colors here refer to the multi-channel cable running to the preamplifiers.

Appendix F (continued)

PLUG II

| <u>Pin</u> | <u>Sensor Wire</u> | <u>Wire Color</u> |
|------------|--------------------|-------------------|
| A          | Ground             | —                 |
| B          | Ground             | —                 |
| C          | 29 <sub>1</sub>    | green             |
| D          | 29 <sub>2</sub>    | black             |
| E          | —                  | —                 |
| F          | 30 <sub>1</sub>    | white             |
| G          | 30 <sub>2</sub>    | red               |
| H          | 28 <sub>2</sub>    | brown             |
| J          | 28 <sub>1</sub>    | green             |
| K          | 27 <sub>2</sub>    | green             |
| L          | 27 <sub>1</sub>    | yellow            |
| M          | 26 <sub>2</sub>    | green             |
| N          | 26 <sub>1</sub>    | white             |
| P          | 22 <sub>2</sub>    | green             |
| R          | 23 <sub>1</sub>    | blue              |
| S          | 23 <sub>2</sub>    | black             |
| T          | 24 <sub>1</sub>    | red               |
| U          | 24 <sub>2</sub>    | blue              |
| V          | 25 <sub>1</sub>    | blue              |
| W          | 25 <sub>2</sub>    | green             |
| X          | 22 <sub>1</sub>    | red               |
| Y          | 21 <sub>2</sub>    | black             |
| Z          | 21 <sub>1</sub>    | yellow            |
| a          | 20 <sub>2</sub>    | red               |
| b          | 20 <sub>1</sub>    | orange            |
| c          | 19 <sub>2</sub>    | black             |
| d          | 19 <sub>1</sub>    | red               |
| e          | 18 <sub>2</sub>    | black             |
| f          | 18 <sub>1</sub>    | white             |
| g          | 17 <sub>2</sub>    | black             |
| h          | 17 <sub>1</sub>    | orange            |
| j          | —                  | —                 |
| k          | 16 <sub>2</sub>    | black             |
| l          | Ground             | —                 |
| m          | 16 <sub>1</sub>    | brown             |

† The 2 subscript refers to the black lead from the sensor, the 1 to the white lead.

‡ The wire colors here refer to the multi-channel cable running to the preamplifiers.